

Transition Metal Complex/Gold Nanoparticle Hybrid Materials

Cristóbal Quintana,^a Marie P. Cifuentes^a and Mark G. Humphrey^{*a}

Received 00th January 20xx,
Accepted 00th January 20xx

DOI: 10.1039/x0xx00000x

Gold nanoparticles (AuNPs) are of considerable interest for diverse applications in areas such as medicine, catalysis, and sensing. AuNPs are generally surface-stabilized by organic matrices and coatings, and while the resultant organic compound (OC)/AuNP hybrids have been explored extensively, they are not suitable for certain applications (e.g. those necessitating reversible redox behaviour and/or long excited-state lifetimes), and they often suffer from low photo- and/or thermal stability. Transition metal complex (TMC)/AuNP hybrids have recently come to the fore as they circumvent some of the aforementioned shortcomings with OC/AuNP hybrids. This review summarizes progress thus far in the nascent field of TMC/AuNP hybrids. The structure and composition of extant TMC/AuNP hybrids are briefly reviewed and the range of TMCs employed in the shell of the hybrids are summarized, the one-phase, two-phase, and post-nanoparticle-synthesis synthetic methods to TMC/AuNP hybrids are discussed and contrasted, highlighting the advantages of variants of the last-mentioned procedure, and the utility of the various characterization techniques is discussed, emphasizing the need to employ multiple techniques in concert. Applications of TMC/AuNP hybrids in luminescence, electrochemical, and electro-optical sensing are described and critiqued, and their uses and potential in imaging, photo-dynamic therapy, nonlinear optics, and catalysis are assessed.

1. Introduction

Hybrid materials (those formed from the combination of two different materials) have attracted ever-increasing attention due to their promise for technological applications in photovoltaics,¹⁻³ energy storage,⁴ catalysis,^{5,6} sensors,⁷ imaging, and medicine.⁸⁻¹⁰ The disparate hybrid materials investigated thus far include mixed-metal oxides, organic compounds (e.g. dyes, pharmacophores, biological probes), or inorganic compounds (e.g. transition metal complexes) embedded in sol-gel matrices or in metal-organic frameworks (MOFs), inorganic particles (e.g. clusters, transition metal nanoparticles, quantum dots) embedded in polymers, inorganic particles coated with organic compounds, and layered organic-inorganic materials. This array of hybrid materials, in which the components bring distinct properties and the combination may offer new or enhanced properties, affords versatility in the design and tailoring of multifunctional devices.^{8,9,11}

In amongst the plethora of possible components of such hybrids, gold nanoparticles (AuNPs) in particular have attracted considerable interest because of their potential use in sensors,^{12,13} nonlinear optics,¹⁴ solar cells,^{15,16} medicine,^{13,17-20} imaging,^{13,19,21,22} and catalysis,²³⁻²⁵ applications in which one or more of their quantum size effects, high surface energies, and high surface-to-volume ratios can be advantageously exploited.²⁶ The properties of AuNPs can be readily tuned

because they depend on the AuNP size and shape as well as the stabilizing ligands present on the surfaces, and all of these can be systematically modified.²⁴ AuNPs possess good stability, they are available from a variety of well-established procedures,^{19,27,28} and they display a rich surface functionalization chemistry with a broad variety of organic matrices and coatings (organic compound/AuNP hybrids), flexibility that has been exploited in the drive to afford novel hybrid multifunctional materials.²⁹⁻³¹

These advantages have resulted in strong interest in organic compound/AuNP hybrids,^{15,32,33} but far fewer reports of transition metal complex (TMC)/AuNP hybrids have appeared. This is surprising, because the hybridization of AuNPs with TMCs may address some of the inherent limitations of organic molecules for applications such as fluorescence lifetime imaging microscopy/mapping (FLIM) (e.g. organic compounds often exhibit short fluorescence lifetimes associated with a lack of triplet states; these impede efficient temporal discrimination in time-gated fluorescence).⁴¹ Moreover, organic dyes are prone to photo and thermal degradation under the experimental conditions required for imaging and microscopy techniques,^{34,35} in contrast, TMCs are generally robust. The structural and electronic properties of TMCs can be fine-tuned by varying the metal atom, the coordination sphere, the coordination geometry, the oxidation state, etc., in contrast to solid-state materials (e.g. perovskites and mixed-metal oxides) and organic compounds (e.g. dyes and fluorophores). Solid-state materials lack the predictability and flexibility of molecular synthesis that is important for facile preparation and tailoring of properties for specific needs.³⁶ In most cases, the performance of solid-state materials depends on bulk properties (e.g. lattice periodicity, structural defects, grain boundaries, purity, etc.) which are variables that are difficult to control by conventional solid-state

^a Research School of Chemistry, Australian National University, Canberra ACT 2601 Australia.

E-mail: mark.humphrey@anu.edu.au

synthesis techniques employing high temperatures and/or pressure.³⁶⁻³⁸ Solid-state materials are often poorly soluble in common organic solvents and are generally suspended in a polymer matrix for studies of their properties, which represents a major limitation due to the need for advanced instrumentation to study this type of material.³⁹ Solid-state materials and quantum dots are generally composed of large amounts of heavy metal atoms; these can be highly toxic, which is a serious limitation for bioimaging and medicinal applications.^{34, 40}

Organic compounds possess a limited range of functional groups with the possibility of reversible oxidation, and they generally exhibit short excited-state lifetimes. Coordination and organometallic TMCs exhibit intense low-energy absorption bands that can be metal-to-ligand charge transfer (MLCT) or ligand-to-metal charge transfer (LMCT) in character;^{41, 42} in particular, TMCs can afford access to low-energy singlet (S_1) and triplet (T_1) MLCT excited states with interesting and potentially useful photophysical properties such as large Stokes shifts, long lived excited-state lifetimes (in the nanosecond to millisecond regime), and moderate quantum yields, as a consequence of strong spin-orbit coupling and strong π -backbonding between the ligands and the metal.^{41, 42} TMCs have therefore been proposed as promising materials for applications in optical limiting (OL),⁴³ organic light emitting diodes (OLEDs), light-electrochemical cells (LECs), solar cells, photodynamic therapy, and imaging and microscopy.^{41, 44} Additionally, TMCs often exhibit one or more reversible metal-centred oxidation processes, and the combination of useful properties make TMCs attractive for applications such as electrochemical sensors,⁴⁵ optical switches and sensors,^{46, 47} and in areas such as catalysis,^{48, 49} energy storage,⁵⁰ polymer science,^{51, 52} and medicine.^{53, 54}

These various advantages of TMCs over organic molecules and solid-state materials also propagate to their AuNP hybrid materials. The combination of TMCs and AuNPs generally results in hybrid materials with good solubility and low toxicity, allowing their use in biological and medicinal applications. The toxicity of TMCs is generally determined by the nature of the coordination sphere, which can be tuned to afford materials suitable for biological applications.⁴¹ Energy and charge transfer can occur between the TMC and AuNP resulting in cooperative effects. The characteristic MLCT transition band usually overlaps with the localized surface plasmon resonance (LSPR) band (collective oscillation of electrons at the surface of the AuNP), giving rise to interesting phenomena such as enhanced singlet oxygen generation,⁵⁵ strong two-photon absorption (2PA),⁵⁶ and high quantum yield.⁵⁷ The hybridization of highly soluble redox active species (e.g. TMCs) with plasmonic nanostructures (e.g. AuNP) affords the prospect of electrochemical sensors with outstanding sensitivity towards the quantification of species of biological importance.⁵⁸ This review of the emerging field of coordination/organometallic TMC/AuNP hybrids contains a summary of the major synthetic approaches to these hybrids, together with the common techniques deployed for characterization, and highlights applications of TMC/AuNP hybrids in optical,⁵⁹

electrochemical,⁵⁸ and electro-optical sensing,⁶⁰ imaging and microscopy,⁶¹ photodynamic therapy (PDT),⁶² nonlinear optics (NLO),⁵⁶ and catalysis.^{63, 64}

2. Hybrid Design

TMC/AuNP hybrids possess a core-shell composition (Fig. 1), with an AuNP core and a shell of surface-stabilizing ligands. The stabilizing ligands are a key component of AuNP-hybrid materials because they define the colloidal stability, the solubility, the charge on the surface, and the potential applications, the last-mentioned depending on additional functionalities that the ligands may contain.²⁴ The ligands in the shells of AuNP hybrids can be classified as auxiliary stabilizing ligands (ASLs) or functionalized stabilizing ligands (FSLs). The ASLs are responsible for the solubility and the colloidal stability of the hybrid; in most cases, they are employed in the synthesis of the AuNPs and are then exchanged (partially or totally) by the FSLs (see section 3.3). The FSLs contain the active components, i.e. the TMCs, that are attached to the AuNP surfaces to provide the functionality (e.g. catalytic, luminescent, redox activity); FSLs can also enhance the solubility.

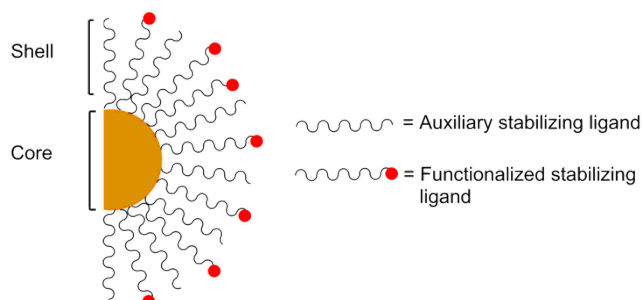


Fig 1. Core-shell model of TMC/AuNP hybrids.

The FSLs can be linear, branched, dendritic, or polymeric in composition, and they generally contain one or more heteroatoms (or building blocks containing one or more heteroatoms) that function as gold anchoring groups (Fig. 2). Linear or rod-shaped molecules have the TMC at one terminus of the molecule and are connected via a spacer to the gold-anchoring group, in order to minimize steric effects. Similar compositions have been reported with dendrons, but in these cases the anchoring groups are located at the dendron foci. When metallated stars or dendrimers are employed in the hybridization of AuNPs, the gold anchoring groups are located in the interior of the dendrimers at the branching or bridging points. In all reports thus far, the metal complexes have been positioned at the periphery of the FSL to minimize steric effects and to maximize the interaction with the environment as well as the surface functionalization.

The solubility of AuNP hybrids is highly dependent on the peripheral functional groups, so the possibility of incorporating either ionic or neutral TMCs can be exploited to tune the AuNP solubility (if the metal complex is ionic, it is likely that the hybrid will be soluble in polar protic solvents, and if neutral it will likely dissolve in organic solvents). For example, surface functionalization of AuNPs with the dicationic Ru(II) complex

$1^{65, 66}$ results in water-solubility, a key requirement for biological probes, and a remarkable improvement in the solubility of metallated phthalocyanines in biological environments is seen following hybridization with AuNPs.⁶⁷ In contrast, the exchange of citrate anions by the cationic Re(I) complexes **5** (e.g. **40** - **43**) results in aggregation of the AuNPs due to neutralization of the charges at the AuNP surfaces.⁶⁸

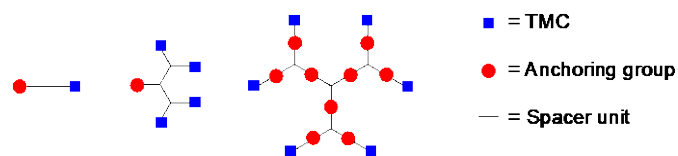


Fig 2. Linear, branched and dendritic architectures of TMC-containing FSLs.

Anchoring groups can be readily incorporated at the metallo- ligands by well-established wet chemistry procedures such as copper-catalyzed alkyne-azide 1,5-cycloaddition (CuAAC), palladium-catalyzed carbon-carbon cross-coupling reactions (e.g. Negishi, Suzuki, Stille), and classic nucleophilic and electrophilic substitution reactions. Commonly used anchoring groups employed in the synthesis of TMC/AuNP hybrids include primary,^{59, 69-71} tertiary,⁷² and quaternary⁷³ amines, carboxylic acids (attached as carboxylates),^{57, 69, 74, 75} 1,2-dithiolanes,^{61, 68, 76} disulfides,⁷⁷ dithiocarbamates,⁷⁸ thioethers,⁷⁹ sulfonates,⁵⁷ and heterocycles such as pyridines,^{65, 80-83} thiophenes,⁵⁶ and 1,2,3-triazoles,^{56, 63, 84, 85} but thiols have been the most intensively investigated by far,⁸⁶⁻¹⁰⁰ because the high binding affinity of gold and sulfur atoms affords long-term stability of the resultant hybrids.¹⁰¹

Extant TMC/AuNP hybrids involve TMC fragments such as $[\text{Ru}(\text{bpy})_3]^{2+}$ (bpy = 2,2'-bipyridine) (**1**),^{66, 102} $[\text{Ir}(\text{ppy})_2(\text{bpy})]^{2+}$ (ppy = 2-phenylpyridine) (**2**),^{61, 103} $[\text{Ru}(\text{terpy})_2]^{2+}$ (terpy = 2,2',6',2''-terpyridine) (**3**),^{104, 105} $[\text{Ru}(\text{phen})_3]^{2+}$ (phen = 1,10-phenanthroline) (**4**),^{70, 80, 105} $[\text{Re}(\text{CO})_3(\text{bpy})(\text{py})]^+$ (py = pyridine) (**5**),^{68, 106, 107} $\text{Rh}(\text{COD})\text{Cl}(\text{py})$ (COD = η^4 -1,5-cyclooctadiene) (**6**),⁸⁷ $\text{RuCl}_2(\text{py})(\text{Cy})$ (Cy = η^5 -*p*-cymene) (**7**),⁸⁷ $\text{Fe}(\text{C}\equiv\text{CR})(\text{dppe})\text{Cp}^*$ (dppe = 1,2-bis(diphenylphosphino)ethane, Cp^* = η^5 -pentamethylcyclopentadienyl) (**8**),⁸⁴ *trans*- $[\text{Ru}(\text{C}\equiv\text{CR})_2(\text{dppe})_2]$ (**9**),⁵⁶ *trans*- $[\text{Pd}(\text{SR})\text{Ph}(\text{PBu}_3)_2]$ (**10**),¹⁰⁸ $\text{RuH}(\text{SR})(\text{CO})(\text{PPh}_3)_3$ (**11**),⁹⁶ ferrocene (**12**),¹⁰⁹ biferrocene (**13**),¹¹⁰ and others,^{85, 109} as well as large macrocycles such as phthalocyanines (**14**) (M = Co, Ni, Zn, Mg, Al) and porphyrins (**15**) (M = Zn, Pd)^{59, 111} because of their physical properties and their robustness (Fig. 3). The good solubility of the TMCs in conventional organic solvents, and thereby the ease of processing, stems from the ancillary ligands such as phosphines,^{88, 101} carbonyls, pyridines, and polypyridines.¹¹²⁻¹¹⁴

3. Synthesis of the Hybrids

TMC/AuNP hybrids have been prepared by standard wet chemistry methods that can be classified as one-phase,^{115, 116} two-phase,¹¹⁷ or post-nanoparticle in nature, the last-mentioned employing ligand exchange,^{98, 118} coulombic and Van der Waals interactions,¹¹⁹ and wet chemistry on the shell of the AuNPs.¹¹⁹ These methods have different features that can be

exploited to afford AuNPs with different shapes and sizes. This section focuses on syntheses of pseudo-spherical particles or nanospheres, which have been the most widely explored TMC/AuNP hybrid shape. The ligands that have been used in the synthesis of AuNP hybrids and the synthetic methods employed are summarized in Tables 2 – 6, with selected FSLs being depicted in Fig. 4.

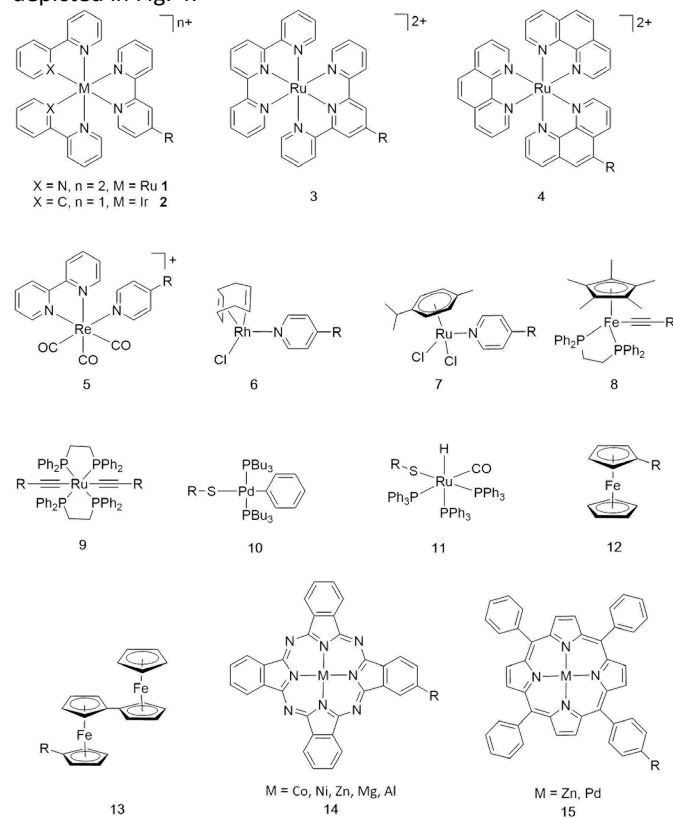


Fig. 3. Structures of TMCs that have been hybridized with AuNPs; the R group denotes the existence of variants.

3.1. One-Phase Method

The one-phase method, commonly known as the Turkevich method, and which was later modified by Frens, involves the reduction of a hot solution of a gold salt in the presence of a stabilizing ligand and a reducing agent. While it has typically afforded AuNPs 10 - 120 nm in diameter,^{115, 116} the size distributions of the AuNPs can be easily tuned within the range 1-10 nm by changing the reducing agent:gold salt ratio.¹²⁰ When the proportion of reducing agent is decreased, the size of the AuNPs increases, while a larger stoichiometric amount of reducing agent results in a decrease in the size of the AuNPs. The one-phase method offers a simple way of preparing AuNPs with a broad size distribution and allows the preparation of larger AuNPs via the seed-mediated growth method.¹²¹ A remarkable aspect of the one-phase method is that the reducing agents (e.g. sodium ascorbate, sodium borohydride, sodium citrate) also function as the stabilizing ligands. AuNPs can be prepared in the presence of a range of metallocene-containing stabilizing agents (ferrocene (**16**) and its derivatives (**17-22**), or ferrocene-containing polymers (**23-25**) and dendrimers (**26**)) without the need for heat, a procedure that

affords well-defined spherical 13 – 45 nm diameter AuNPs.^{63, 84, 85, 110, 122} A mixture of TMC and ASL can be used to prepare TMC/AuNPs with improved properties using the one-phase method. For example, a mixture of thiol-tethered phthalocyanine (**74**, **92**) and thiol-appended poly(ethylene glycol) results in TMC/AuNP hybrids with enhanced solubility in aqueous solutions.^{123, 124} However, the one-phase method is not a broadly applicable procedure because certain coordination and organometallic complexes (e.g. metal alkynyl complexes⁵⁶) and organic building blocks (e.g. thiophene¹²⁵) are sensitive to the acidic/basic and/or oxidizing/reducing environments employed.

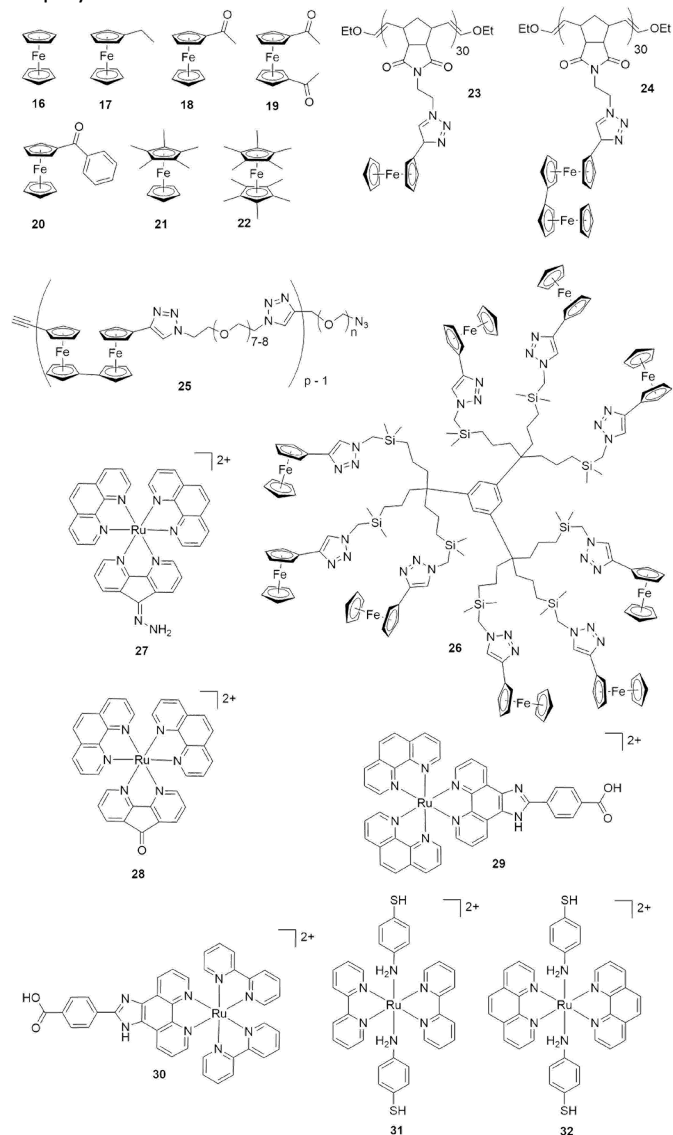


Fig. 4. Structures of FSLs 16 – 32.

3.2. Two-Phase Method

Due to the aforementioned shortcomings with the one-phase method, attention turned to the two-phase method. The two-phase method pioneered by Brust and Schiffrin employs a phase-transfer catalyst (PTC), such as tetra-*n*-octylammonium bromide (TOAB), in an organic solvent (e.g. toluene, dichloromethane) to transfer a gold salt (Au^{3+}) from an aqueous

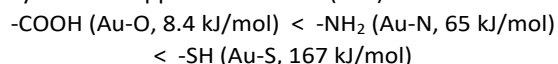
solution to the organic phase.¹¹⁷ The stabilizing agent is then added (*n*-dodecanethiol was employed in the original work, but more recently, a panoply of sulfur- and amine-based ligands have been used), followed by a mild reducing agent, such as NaBH_4 , to generate the thiol-coated AuNPs. In an analogous fashion to the one-phase method, varying the thiol:gold salt ratio results in AuNPs with differing size distributions: a high thiol:gold ratio leads to small diameter AuNPs (< 2 nm), while a low thiol: gold salt ratio leads to larger AuNP core sizes (ca. 5 nm). This method affords highly stable small to ultra-small AuNPs with diameters in the size range 1 – 5 nm (and with a narrow size distribution) that can be isolated by precipitation and then re-dispersed in common organic solvents. Degradation of the TMC can occur due to the strongly acidic and oxidizing environment employed in the two-phase method, but this problem can be avoided by using an excess of the PTC, thereby forming a more persistent amphiphilic micellar structure in the organic solvent that effectively encapsulates and isolates the ionic species.^{56, 125}

3.3. Post-Nanoparticle-Synthesis Methods

Several methods for the introduction of TMCs after AuNP synthesis have been deployed, the general routes being summarized below, and examples being depicted in Scheme 1.

3.3.1. Ligand Place-Exchange Reaction. The ligand place-exchange reaction (LP-ER) method (or "ligand exchange method") is a post-nanoparticle-synthesis surface functionalization technique based on the replacement of the stabilizing ligands at the surface of AuNPs (Scheme 1A).⁹⁸ This method allows precise control over the size of the core and composition of the shell, and is one of most common methods used for the preparation of TMC/AuNP hybrids. The AuNPs are prepared either by the one-phase or the two-phase methods, and the ASLs are then replaced by FSLs via a ligand exchange reaction. The nature of the ASLs is crucial, as the ASLs must possess the following three characteristics to be suitable for the synthesis of TMC/AuNP hybrids: i) good solubility in conventional solvents, ii) high stability in solution and solid state, and iii) the anchoring groups must have equal or lower binding affinity than the FSL for gold. Good ligand solubility is required to disperse the nanomaterial in a suitable solvent, high stability of the ligands is required to maintain the shape and size distribution of AuNPs over time, crucial for processability purposes, while the third-mentioned, directly related to the binding strength of the anchoring group to the AuNP surface, is needed for efficient replacement of ASLs by FSLs. ASLs employed in the synthesis of TMC/AuNP hybrids include citrate,^{69, 105} TOAB,^{104, 126} *n*-dodecylamine, *n*-dodecanethiol, *n*-hexanethiol,^{86, 87, 127} mercaptooctanoate, PEGylated thiols (thiol-containing poly(ethylene glycol)s),^{128, 129} and more sophisticated surfactants such as tiopronin (*N*-(2-mercaptopropionyl)glycine),¹³⁰ *N,N*-trimethyl(undecylmercapto)ammonium,¹³⁰ ZonylTM fluorosurfactants (FSAs),^{61, 102, 103, 131} and TritonTM X-100 (a poly(ethylene glycol) derivative).⁷³ The difference in binding strength and size of the ligands determines the reaction rate and the degree of surface functionalization of the shell of the

AuNP hybrid.⁹⁸ The functionalization of the shell can be quantitative or partial, and this can be easily controlled by exploiting differences in the binding strengths of FSL-Au and ASL-Au, available from scanning tunnelling microscopy (STM) studies of self-assembled monolayers of alkyl amines, thiols and carboxylic acids supported on an Au(111) surface:¹³²



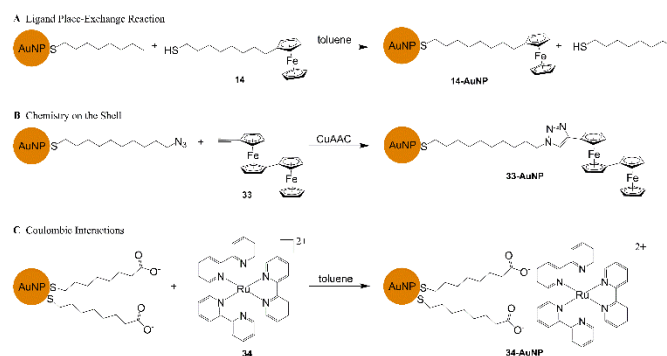
For example, if quantitative ligand place-exchange is required, an ASL containing an $-\text{NH}_2$ or $-\text{COOH}$ group can be employed initially, to be replaced by an SH-containing FSL. Partial ligand exchange is targeted when a lower degree of surface functionalization is required, or when the ligand exhibits poor solubility or compatibility with the surface of the AuNP. Whenever partial ligand place-exchange is sought, the ASL should have a binding strength approximately equal to the FSL. The rate of the ligand exchange reaction decreases as the length or bulkiness of the auxiliary ligand increases.

It is important to account for the surface charge of the AuNP hybrid when carrying out the ligand exchange reaction. Electrostatic and coulombic interactions between charged species can lead to modification or aggregation of the AuNP cores during LP-ERs. For example, structural modifications of the AuNPs are observed during exchange of citrate ASLs by ruthenium(II) bipyridyl complexes containing anchoring groups with low affinity for gold (e.g. amine (**27**), ketone (**28**) or carboxylic acid (**29**, **30**)); in contrast, no structural variations are observed in this system with thiol anchoring groups (**31**, **32**),⁶⁹ although aggregation of 15 nm diameter AuNPs occurs during ligand exchange of citrate anions by thiol-tethered $[\text{Ru}(\text{phen})_3]^{2+}$ complexes (**69-71**).¹⁰⁵ The use of surfactants such as ZonylTM and TritonTM X-100 can reduce this aggregation of the AuNPs through surface charge stabilization and core isolation, resulting in a high loading of FSLs.^{61, 73, 102, 103, 131} The use of mixed layers of stabilizing ligands has also been shown to prevent precipitation of triethylene glycol thiol-coated AuNPs, during a LP-ER between *n*-triethylene glycol thiol and *n*-alkylthiol-tethered $[\text{Ru}(\text{bpy})_3]^{2+}$ cationic species (**35**).¹³³

Overall, the ligand exchange method has advantages: it permits the use of a pre-determined AuNP core size, and it is the method of choice when the TMC employed is sensitive to high temperatures (one-phase method), mild reductants, or strong acidic or oxidizing agents (one- and two-phase methods).

3.3.2. Direct Covalent Chemistry on the Shell. TMCs have also been introduced at the periphery of the AuNP hybrid shell via chemical reactions at AuNP-bound functional groups, e.g. via copper-catalyzed azide-alkyne coupling (CuAAC) or by simple coordination chemistry (Scheme 1B). CuAAC has been employed to attach a broad variety of functional moieties of biological interest such as proteins, peptides and DNA to AuNPs; however, reports of CuAAC being used to attach TMCs to AuNPs are limited. Ferrocenyl-containing species (e.g. **33**, Scheme 1B) have been linked to the shell of AuNPs under CuAAC conditions,¹³⁴ but this procedure necessitates strong gold-ligand attachment; aggregation of the AuNPs has been observed when CuAAC is employed at ligands attached to AuNPs through weak anchoring groups such as carboxylate.¹³⁵

Coordination chemistry on the shell of the hybrid is also relatively unexplored compared to the methods described in Sections 3.1, 3.2 and 3.3.1: among limited examples, rhenium(I) carbonyl species have been successfully coordinated to the carboxylated periphery of AuNPs,¹³⁶ and the chloro ligand of $\text{RuHCl}(\text{CO})(\text{PPh}_3)_3$ has been displaced by pendant thiol groups at triazine-coated AuNPs.⁹⁶



Scheme 1. Selected examples of post-nanoparticle-synthesis methods: A) ligand place-exchange, B) chemistry-on-the-shell syntheses, and C) coulombic interactions.

3.3.3. Coulombic Interactions. Self-assembly in solution of a charged TMC (usually cationic) and charged functional groups at the periphery of an AuNP (carboxylates, quaternary amines, and ionic counter ions (e.g. citrate anions)) is a procedure that was employed in early reports of TMC/AuNP chemistry (Scheme 1C).^{130, 137} This method has some flexibility (the TMCs assembled at the surface of the AuNPs can be readily displaced by other cations in solution), but it has since been replaced by synthesis methods affording more robust TMC-AuNP linkages.

4. Characterization Techniques

TMC/AuNP hybrids have been characterized using a range of techniques, including NMR (Fig. 5A), IR (Fig. 5B), and Raman spectroscopy (Fig. 5C), energy dispersive X-ray spectroscopy (EDX) (Fig. 5D), thermogravimetric analysis (TGA), dynamic light scattering (DLS) (Fig. 5E), X-ray photoelectron spectroscopy (XPS) (Fig. 5F), UV-Vis spectroscopy (Fig. 5G), powder X-ray diffraction (PXRD) (Fig. 5H), zeta-potential studies (Fig. 5I), scanning electron microscopy (SEM), transmission electron microscopy (TEM) (Fig. 5J), inductively coupled plasma (ICP) optical emission spectroscopy (OES), and mass spectrometry (MS) (Fig. 5K). Each technique provides useful insight into one or more of the size distribution, stability, surface functionalization, composition, and morphology of the nanomaterial; the information obtained from each technique is summarized in Table 1. The hybrid nanomaterials should be characterized using several complementary techniques in concert, in order to remove ambiguities associated with the use of a single technique, and to have a clear understanding of the material properties. A comprehensive review regarding conventional and advanced techniques to characterize a diverse array of nanomaterials has appeared recently.^{138, 156}

ARTICLE

Table 1. Characterization Techniques Employed with TMC/AuNP Hybrids.

Technique	Information	Ref
UV-Vis-NIR spectroscopy	Size distribution Concentration of AuNPs Kinetics of the AuNP-hybrid synthesis and ligand exchange reactions	139
Transmission and scanning electron microscopy (TEM and SEM, respectively), atomic force microscopy (AFM)	Size distribution of the core Morphology of the hybrids	140, 141
X-ray photoelectron spectroscopy (XPS)	Oxidation states of the elements Binding modes of the anchoring groups to the AuNP surface	142
Dynamic light scattering (DLS)	Hydrodynamic diameter Colloidal stability of the hybrid material Polydispersity index	143
Energy dispersive X-ray spectroscopy (EDX)	Determination of the elemental composition	138
NMR spectroscopy	Progress of the AuNP hybrid synthesis Determination of the different ligands present in the shell	144
Inductively coupled plasma-mass spectrometry/optical emission spectroscopy (ICP-MS/OES), thermogravimetric analysis (TGA)	Elemental composition of the hybrids Stoichiometry of the surface functionalization (AuNP:ligand ratio)	145- 147
FT-IR spectroscopy	Progress of the AuNP synthesis Au-E signatures (E = S, N, O)	148- 152
Powder X-ray diffraction	Determination of crystal structures	153
Zeta potential	Colloidal stability of the hybrids at different pH values Size distribution of the hybrids Surface charge	154
Raman scattering	Binding modes of the ligands to the AuNP surface	155, 156

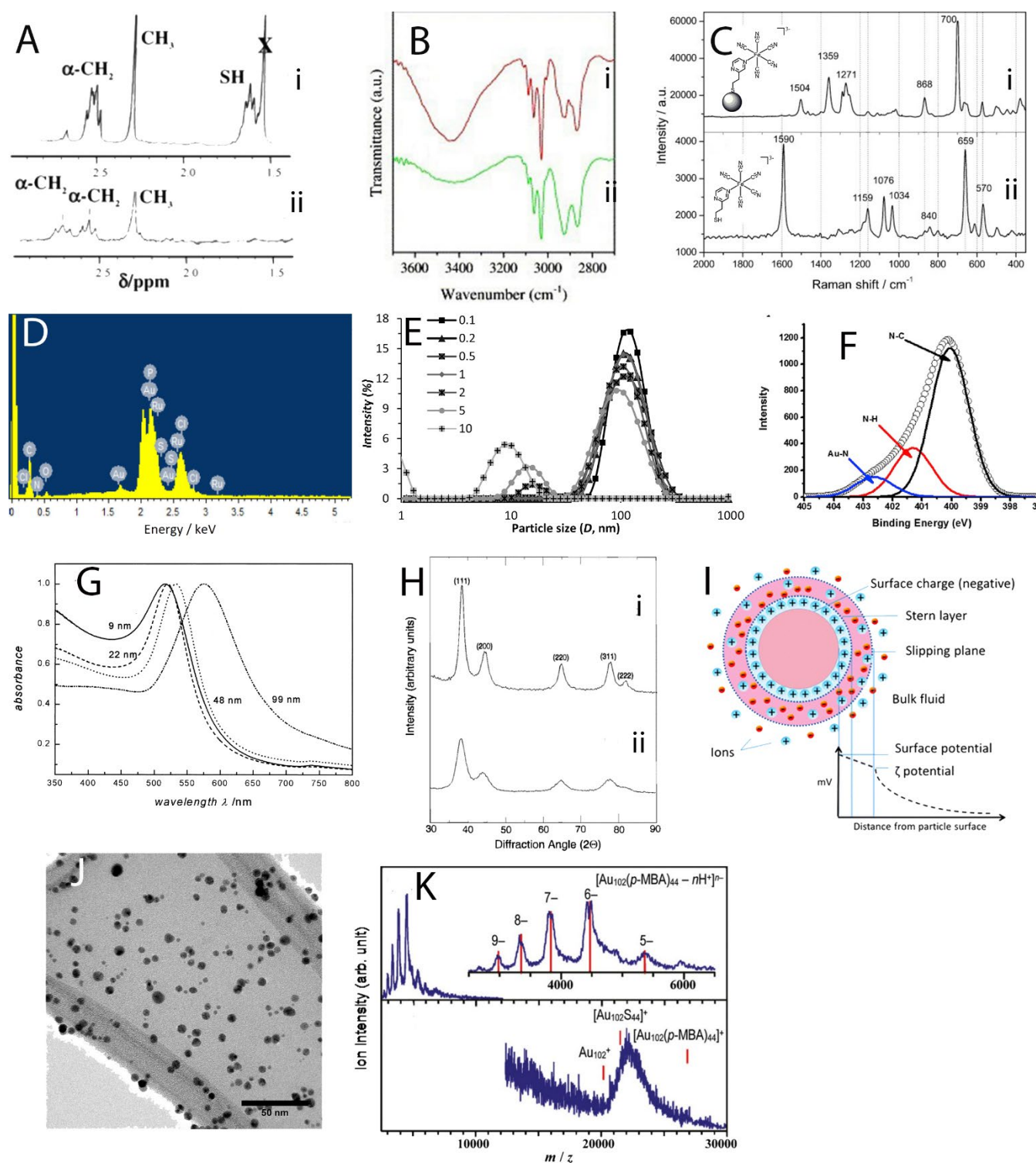


Fig. 5. Representative images of techniques employed in the characterization of TMC/AuNP hybrids: A) ^1H NMR spectra displaying the presence and the absence of the resonance of the thiol group (-SH) of a tris(bipyridyl)ruthenium(II) derivative before and after attachment to AuNPs. Reprinted with permission from ref. 133. Copyright 1996 American Chemical Society. B) FT-IR spectra showing the difference in O-H stretching vibration mode of the free FSL (i) and the FSL attached to the AuNP surface (ii). Reprinted with permission from ref. 152. Copyright 2007 Elsevier. C) Raman spectra of $[\text{Fe}(\text{CN})_5(\text{pyrazine-2-ethanethiolate})]^{3-}$ attached to AuNPs (i) and $[\text{Fe}(\text{CN})_5(\text{pyrazine-2-ethanethiolate})]^{3-}$ (ii) attached to AuNPs. Reprinted with permission from ref. 119. Copyright 2010 Creative Commons. D) EDX spectrum of an organoruthenium complex attached to the surface of AuNPs. Reprinted with permission from ref. 96. Copyright 2016 American Chemical Society. E) DLS plot of the size distribution of organic-coated AuNPs. Reprinted with permission from ref. 157. Copyright 2017 Creative Commons. F) XPS images showing the different binding energies (N-Au, N-H and N-C) of a metallophthalocyanine attached to the surface of an AuNP. Reprinted with permission from ref. 158. Copyright 2016 Elsevier. G) UV-Vis spectra showing the LSPR of AuNPs of various sizes. Reprinted with permission from ref. 159.

Copyright 1999 American Chemical Society. H) Powder X-ray diffraction patterns of amine-capped AuNPs with average size distribution of 6.3 nm (i) and 3.7 nm (ii). Reprinted with permission from ref. 160. Copyright 1996 American Chemical Society. I) Schematic representation of zeta potential showing the ionic concentration and potential differences as a function of distance from the charged surface of a particle suspended in a medium. Reprinted with permission from ref. 161. Copyright 2012 Royal Society of Chemistry. J) TEM image of organoruthenium-coated AuNPs. Reprinted with permission from ref. 56. Copyright 2019 American Chemical Society. K) ICP-MS spectrum of $[\text{Au}_{102}(\text{p-MBA})_{44}]$ (p-MBA = p-mercaptobenzoic acid). Reprinted with permission from ref. 162. Copyright 2014 Elsevier.

An estimate of the formula weight (FWt, in grams per mole) of TMC hybrids is needed to obtain concentration-related molecular (nanomaterial) properties (such as molar absorptivity coefficients, two-photon absorption cross-sections, etc.) and other useful merit figures that allow comparison between species with disparate compositions and architectures. The FWt of a hybrid can be estimated from the sum of the average number of gold atoms per AuNP core (N_{Au}) and the average number of complexes (N_{complex}) in the shell (Eq. 1), assuming there are no other stabilizing ligands present:

$$\text{FWt} = N_{\text{Au}} \times \text{AtWt}_{\text{Au}} + N_{\text{complex}} \times \text{FWt}_{\text{complex}} \quad (\text{Eq. 1})$$

N_{Au} , the number of Au atoms per AuNP, can be estimated according to Eq. 2 (where ρ is the density of gold, D is the diameter of the AuNP core in nm, AtWt_{Au} is the atomic weight of gold, and N_{A} is Avogadro's constant). Eq. 2 can be reduced to Eq. 3:¹⁶³

$$N_{\text{Au}} = \frac{\pi(\rho D^3)}{6 \text{AtWt}_{\text{Au}}} N_{\text{A}} \quad (\text{Eq. 2})$$

$$N_{\text{Au}} = 30.8960D^3 \quad (\text{Eq. 3})$$

where the average AuNP diameter D can be obtained from TEM or SEM analysis and N_{complex} can be estimated using N_{Au} as reference together with the Au:metal ratio, the latter determined from ICP-OES/MS analysis or any other elemental analysis technique. The error associated with the FWt can be propagated into other merit figures by using standard error propagation statistical analysis.¹⁶⁴

5. Applications

5.1 Sensing

5.1.1. Optical sensing. AuNPs can either enhance or decrease (quench) the luminescence properties of molecules located in close proximity, and this characteristic has been exploited for sensing applications.¹² Fluorescence quenching occurs at short distances (ca. 0-5 nm), while spatial variation of the incident light field (ca. 0-15 nm) and changes in the radiative decay rates (ca. 0-20 nm) are seen over longer distances.¹⁶⁵

Late transition metal complexes with closed-shell electronic configurations can exhibit long-lived excited-state lifetimes ($\tau \approx 100$ ns to ms) and afford low energy singlet (S_1) and triplet (T_1) MLCT transition bands as a result of strong spin-orbit coupling via intersystem crossing.¹⁶⁶ These have been shown to be promising probes for time-gated luminescence, because their long lifetimes and large Stokes shifts (10 – 100 nm) facilitate signal discrimination from self-quenching of the luminescence of the probe and the autofluorescence of the biological samples

(which is usually short lived, much less than 10 ns), thereby enabling fluorescence lifetime imaging microscopy and mapping (FLIM).^{41, 61}

In view of the attractive properties of AuNPs and TMCs, their hybrids have been proposed for sensor applications, since a greater degree of signal quenching would be expected for molecules exhibiting larger luminescence intensity due to the proximity of AuNPs. The resulting sensing devices will show enhanced sensitivity, as suggested by the Stern-Volmer equation (Eq. 4),⁹³ which relates fluorescence intensity of an emitter (e.g. a TMC) in the presence (I) and absence (I_0) of a quencher (e.g. a AuNP) to the bimolecular quenching constant (k_q), the non-quenched lifetime (τ_0) and the quantum yield (Q) of the fluorophore:

$$\frac{I_0}{I} = 1 + k_q \tau_0 [Q] \quad (\text{Eq. 4})$$

It is clear from Equation 4 that compounds with longer excited-state lifetimes are (unsurprisingly) quenched more readily than compounds possessing shorter excited-state lifetimes. TMCs usually possess considerably longer excited-state lifetimes than organic dyes due to spin-orbit coupling, so TMCs with long-lived excited states are anticipated to display higher sensitivity in optical sensing devices when attached to a AuNP.

Resonance energy transfer (RET) is an important mechanism for quenching the fluorescence of molecules surrounding AuNPs.^{13, 167} Plasmon oscillations relax non-radiatively through electron-electron collisions, electron-lattice phonon and electron-surface interactions, leading to AuNP absorption processes.^{13, 167} The distance between the fluorophore and the AuNP has a strong influence on the fluorescence intensity and fluorescence lifetime.¹⁶⁸ The latter are governed by the rate of energy transfer (k_T), which is given by Eq. 5:⁹³

$$k_T = \frac{1}{\tau_0} \left(\frac{R_0}{r} \right)^6 \quad (\text{Eq. 5})$$

where R_0 is the Förster radius and r is the distance from the fluorophore to the AuNP surface. From Eq. 5, it can be seen that fluorophores in close proximity to the AuNP surface will exhibit a larger k_T than those positioned further away, resulting in stronger quenching of the emission and reduced lifetime of the luminophore. Assessing RET in chromophore/AuNP hybrids is highly effective for determining interparticle distances.¹⁶⁹

Recent studies of optical sensors containing TMC/AuNP hybrids have involved the displacement/attachment of a fluorophore from/to the surface of an AuNP by means of LP-ER, or a spatial rearrangement at the AuNP surface resulting from a chemical stimulus recovering/quenching the luminescence of the TMC. Table 2 shows TMC/AuNP hybrids explored as optical sensors.¹¹⁹ Early examples exploited electrostatic interactions between $[\text{Ru}(\text{bpy})_3]^{2+}$ (**34**) and surface-charged 1.8 – 2.2 nm AuNPs with anionic (carboxylate, **34-AuNP-1**) and cationic (quaternary amine, **34-AuNP-2**) functional groups on the periphery of the shell, which resulted in a 70 % quenching of the luminescence.¹³⁰ The electrostatic interaction is reversible

because the $[\text{Ru}(\text{bpy})_3]^{2+}$ luminescence was recovered on addition of cations such as K^+ , Ca^{2+} , and NEt_4^+ . To understand the mechanism of quenching by the AuNP hybrids, the fluorescence of $[\text{Ru}(\text{bpy})_3]^{2+}$ (**34**) has been assessed before and after hybridization with 10 nm diameter (mercapto)octanoate-coated AuNPs with the use of time-correlated single-photon counting (TCSPC).¹³⁷ The main quenching process in the hybrid **34-AuNP-3** is believed to involve electron-transfer from the MLCT excited-state to the surface of the AuNP, followed by back electron-transfer. The lifetime decay plots of the hybrids reveal a tri-exponential decay attributed to i) the complex adsorbed directly to the surface of the AuNP, ii) the adsorbed complex interacting electrostatically with the stabilizing ligands at the surface of the AuNP, and iii) the free complex, and this collective behaviour affords a method of characterizing the nature of the adsorbates at the surface of AuNPs. Nanosecond transient absorption spectroscopy and TCSPC studies suggest that the strong quenching seen when the *n*-heptanethiol-tethered ruthenium(II) tris-bipyridyl derivative (**35**) is attached to triethylene glycol-coated AuNPs corresponds to a concentration-dependent electron-transfer between the adjacent ruthenium(II) tris-bipyridyl moieties present in the shell of the TMC-AuNP hybrid (**35-AuNP**).¹³³

Differences in AuNP core diameters in the range 10 – 100 nm have little to no influence on the quenching efficiencies of the metal-containing chromophores.^{59, 61, 102} In contrast, the degree of luminescence quenching is highly dependent on the distance of the chromophore from the AuNP surface, and is related to the distance-dependent increase in rate of nonradiative decay that results from electron- or energy-transfer (k_{ET}) from the chromophore to the AuNP core.⁹³ The emission of the ruthenium(II) tris-bipyridyl derivative **36** is strongly quenched when closely bound to the surface of 17, 60, and 120 nm AuNPs (estimated radial distance 0.7 nm from the AuNP surface), whereas an increase in luminescence is observed when the length of the spacing unit between the complex and the anchoring group is increased from compound **36** (**36-AuNP-1-3**, QY = 0.02) to **37** (**37-AuNP-1-3**, QY = 0.05, radial distance 1.6 nm) and on to **38** (**38-AuNP-1-3**, QY = 0.09, radial distance 2.5 nm).¹⁰²

Hybrids of the adamantane-tethered ruthenium(II) tris-bipyridyl derivative **39** or the rhenium(I) tricarbonyl polypyridyl derivative **40** and β -cyclodextrin-capped 13 nm diameter AuNPs (**39-AuNP** and **40-AuNP**, respectively) display dual sensing properties (Fig. 6).¹⁰⁶ In the former, the bpy ligands are connected through *n*-alkyl spacer groups to adamantane fragments which participate in host-guest interactions with the β -cyclodextrin pockets on the surface of the AuNPs. The AuNP hybrids possess steroid- and esterase-sensing capability by means of fluorescence recovery; this is effected either by displacement of the complexes (steroid sensing) or by cleavage of the ester bond present in the bpy ligand of the complexes (esterase sensing). Similar esterase sensing studies of AuNPs hybridized with Re(I) complexes (**41-AuNP**, **42-AuNP**, **43-AuNP**, **44-AuNP**) have shown that a greater spectral overlap of the localized surface plasmon resonance (LSPR) absorption band and the emission band of the fluorophore (and thereby enhanced energy transfer) results in higher quenching efficiency,⁶⁸ an outcome also seen with the 1,2-dithiolane-tethered ruthenium(II) tris-bipyridyl derivative (**45**) and the rhenium(I) tricarbonyl polypyridyl derivative (**46**).¹⁰⁶ Quenching from Förster resonance energy-transfer (FRET) in similar

esterase-sensing systems that are linked by a covalent bond to the AuNP surface is also possible;¹⁰⁷ this has been exploited in AuNPs coated with $[\text{Ru}(\text{bpy})_3]^{2+}$ moieties labelled with DNA that have been used as luminescence probes for the detection of deoxyribonuclease (DNase).¹⁷⁴

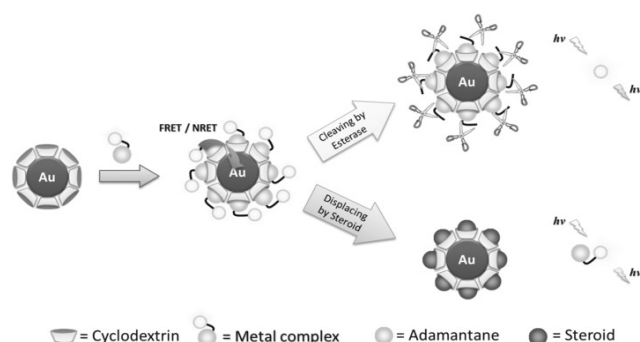


Fig. 6. Schematic representation of esterase and steroid sensing by noncovalent $\text{Ru}^{\text{II}}/\text{Re}^{\text{I}}$ -functionalized β -cyclodextrin/AuNP hybrids **39-AuNP** and **40-AuNP**. Reprinted with permission from ref. 106. Copyright 2015 Wiley VCH.

Even more complex designs have been explored for biomolecule recognition. For example, streptavidin (SA)/bovine serum albumin (BSA)/PEG/AuNP hybrids have been employed as molecular recognition sensors for the biotin-functionalized PEGylated ruthenium(II) tris-bipyridyl derivative (**47**) or palladium(II) porphyrin (**48**) (**47-AuNP** and **48-AuNP**, respectively) (Fig. 7).⁵⁹ Luminescence quenching efficiencies of ca. 80 % are observed after recognition of the complexes by the SA/BSA/PEG/AuNP at an estimated radial distance of 4 nm.

Overall, the degree of quenching induced by the AuNP core in such sensing applications is highly dependent on i) the position of the LSPR band compared to the emission band of the TMC (in general, a better spectral overlap between these two bands favours quenching due to energy- or electron-transfer to the AuNP core in the excited-state), ii) a shorter radial distance, and iii) non-covalent interactions (which afford a stronger degree of quenching if the AuNP surface and the TMC are in close proximity). All three factors are important in the application of fluorescent sensors and labels, and all must be considered when designing luminescent AuNP-hybrid materials.

5.1.2. Electrochemical Sensing. Ferrocene and its derivatives display exceptional stability in their accessible redox states and have consequently been explored as electrochemically-responsive modules in molecular electronics and sensor applications.¹⁷⁵ AuNPs can function as electron shuttles in solution or when supported at an electrode surface, because they can stabilize variable charge at their periphery; as a result, AuNPs have potential in nano-electrodes applications. Hybridization of AuNPs with redox-active ferrocenyl moieties is therefore an attractive prospect (Table 3). For example, *n*-octylthiol-coated AuNPs have been partially surface-functionalized with ω -thiooctylferrocene (**49**), and the ferrocene units employed as a reference in the calculation of the diffusion constant and the capacitance of the AuNP core of the hybrid **49-AuNP**.^{176, 177} The charging capacitance of fully ferrocenylated hexylthiolate-stabilized AuNPs (**50-AuNP-n**, $n = 1-5$) increases considerably when several ferrocene groups are present in the shell (allowing a larger amount of charge per volume); these hybrids can transfer up to 60 electrons per ω -thiohexylferrocene/AuNP (hybrid core diameters ca. 2.2 ± 0.2 nm).¹⁷⁹ The capacitance properties are highly dependent on hybrid size (core + shell), with higher capacitance per unit

volume being found on decreasing the (core + shell) diameter.¹⁷⁹

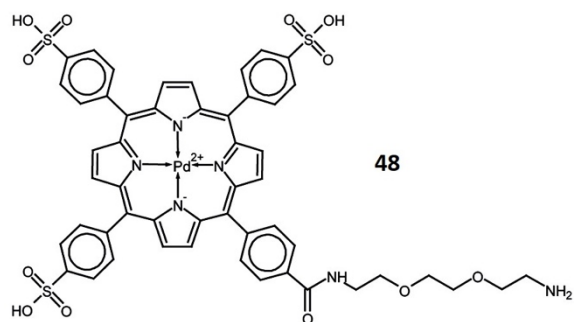
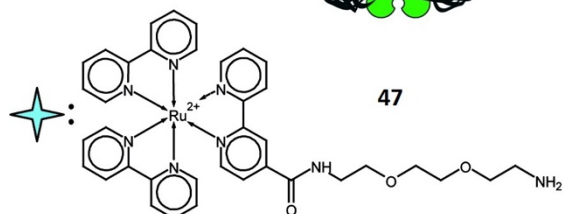
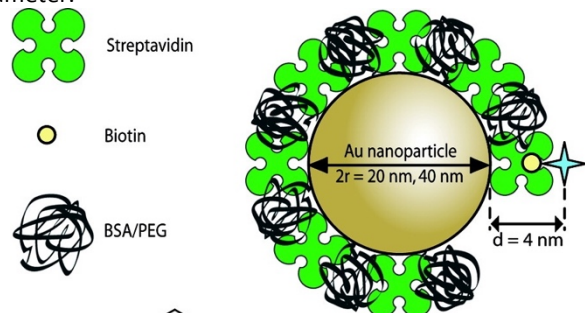
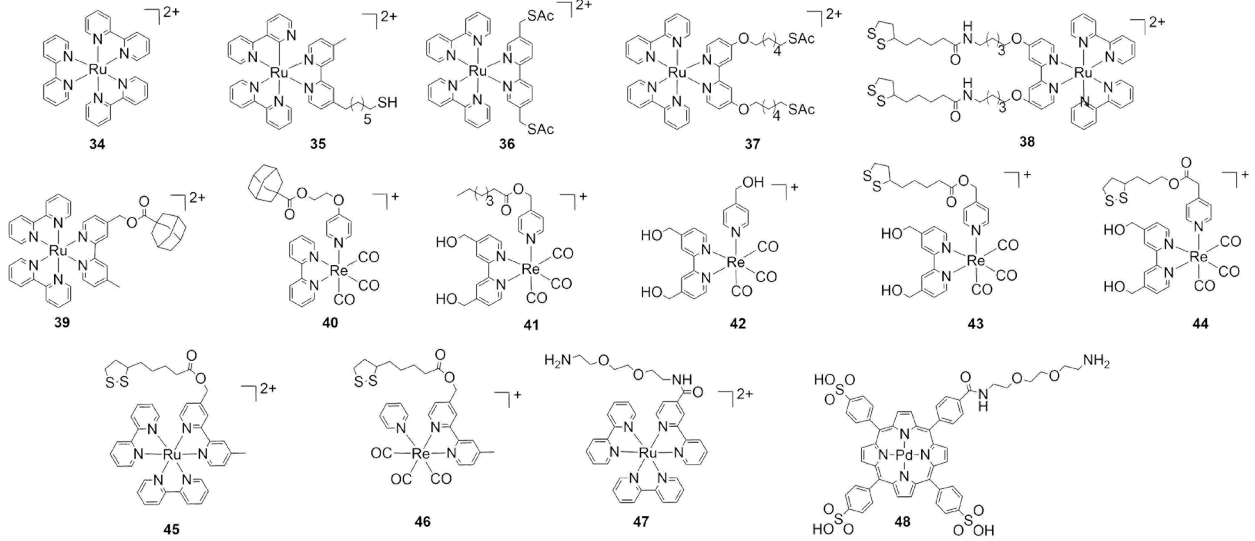


Fig. 7. Phosphorescent metal complexes **47** and **48** attached via streptavidin-biotin recognition to 20 and 40 nm diameter AuNPs; the residual AuNP surface is sealed with either BSA or PEG. The phosphors are ca. 4 nm from the AuNP surface. Reprinted with permission from ref. 59. Copyright 2007 American Chemical Society.

Table 2. Synthesis, ASLs, Size Distributions, and Linear Optical Properties of Hybrids Incorporating FSLs **34** - **48**.


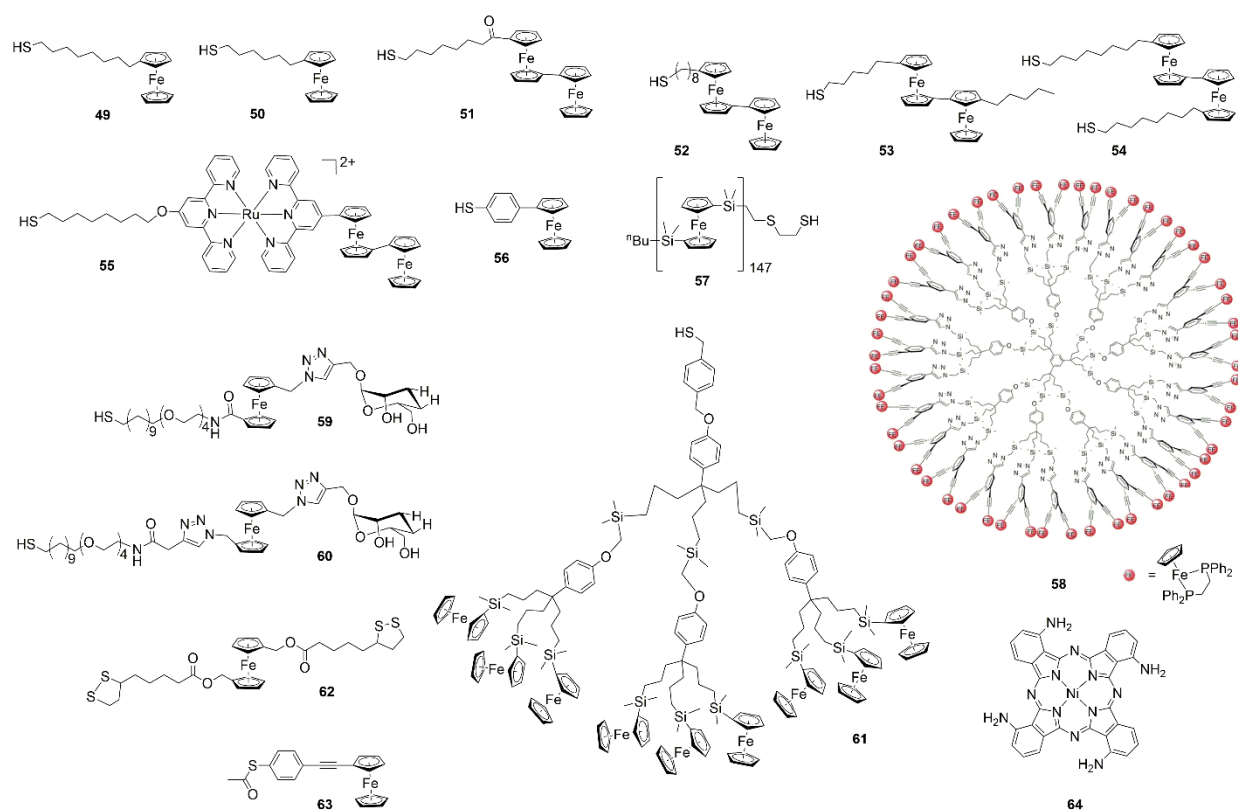
The figure displays the chemical structures of 15 different functionalized single-layered ligands (FSLs), labeled 34 through 48. These ligands are based on various metal centers (Ru, Re, Pd) coordinated by nitrogen-containing ligands. They feature diverse functional groups such as thiols, thioesters, hydroxyl groups, and amine groups, which are used for hybridization with gold nanoparticles (AuNPs).

Compound	Synthesis ^a	ASL ^b	Size (nm)	λ_{\max} (nm) ^c	λ_{em} (nm) ^d	Φ ^e	τ (ns) ^f	Ref
34				452	628	0.33	16 000	130, 170
34-AuNP-1	Cl	N-2-NPG	1.8	Not specified	620	Not specified	Not specified	130
34-AuNP-2	Cl	N,N-TMUA	2.2	Not specified	620	Not specified	Not specified	130
34-AuNP-3	Cl	Mercaptooctanoic acid	10	Not specified	Not specified	Not specified	605	134
35				453	617	0.070	960	133
35-AuNP	LP-ER	Triethylene glycol thiol	4.5	453	617	Not specified	960 (30 %), 4.2 (70 %)	133
36				517	610	0.02	420	171
36-AuNP-1	LP-ER	Zonyl FSA	17	521 (LSPR)	650	0.02	470	102
36-AuNP-2	LP-ER		60	537	650	0.02	470	
36-AuNP-3	LP-ER		120	569	650	0.02	470	
37				462	650	0.02	240	102
37-AuNP-1	LP-ER	Zonyl FSA	17	522	650	0.05	340	102
37-AuNP-2	LP-ER		60	536	650	0.05	340	
37-AuNP-3	LP-ER		120	569 (LSPR)	650	0.05	340	
38				461	645	0.02	280	172
38-AuNP-1	LP-ER	Zonyl FSA	17	520	650	0.09	480	102
38-AuNP-2	LP-ER		60	537	650	0.09	480	
38-AuNP-3	LP-ER		120	569 (LSPR)	650	0.09	480	
39				455	632	0.059	690	106
39-AuNP	SA	Cyclodextrin	3.5	~ 515 (LSPR)	632	0.0059	407	106
40				355	563	0.037	220	106
40-AuNP	SA	Cyclodextrin	3.6	~ 515 (LSPR)	563	0.0031	155	106
41				347	546	11.00	120	68
41-AuNP	LP-ER	Sodium citrate	18 ± 4.6	~ 640	550	3.68	Not specified	68
42				350	544	16.00	140	68
42-AuNP	LP-ER	Sodium citrate	18 ± 4.6	~ 640	550	2.79	Not specified	68
43				346	542	9.00	80	68
43-AuNP	LP-ER	Sodium citrate	18 ± 4.6	611	550	1.35	Not specified	68
44				345	542	10.00	90	68
44-AuNP	LP-ER	Sodium citrate	18 ± 4.6	611	550	1.00	Not specified	68
45				456	625	0.05	560	106
45-AuNP	LP-ER	Dimethylaminopyridine	5.4	524	625	0.0056	359 (72.3 %), 7.81 (27.7 %)	106
46				346	563	0.011	207	106

46-AuNP	LP-ER	Dimethylaminopyridine	5.2	523	563	0.0011	112	106
47				452	628	0.027	380	59
47-AuNP	LP-ER	Streptavidin and BSA glycol	20	523 (LSPR)	628	0.0050	44	59
			40	523 (LSPR)	628	0.0054	42	
48				522	Not specified	0.028	450 000	59, 173
48-AuNP	LP-ER	Streptavidin and BSA	20	523 (LSPR)	Not specified	0.0056	82 000	59

[a] Cl = coulombic interactions, LP-ER = ligand place-exchange reaction, SA = self assembly; [b] N-2-MPG = *N*-(2-mercaptopropionyl)glycine (tiopronin), N,N-TMUA = *N,N*-trimethyl(undecylmercapto)ammonium, BSA = bovine serum albumin; [c] absorption maximum; [d] emission maximum; [e] quantum yield; [f] emission lifetime.

Table 3. FSL Structures, AuNP Hybrid Synthesis, ASLs, Size Distributions, and Applications of Hybrids Incorporating FSLs **49 – 64**. Complex **58** reprinted with permission from ref. 84. Copyright 2014 Springer Nature.



Compound	Synthesis	ASL	Size (nm)	Application	Ref
49-AuNP	LP-ER ^a	<i>n</i> -Octanethiol	1.0 – 1.3	Fundamental electrochemical studies and deposition on electrodes	176-178
50-AuNP-1	Two-phase method	None	1.4 ± 0.2 1.6 ± 0.2 2.0 ± 0.2 2.2 ± 0.2	Fundamental electrochemical studies	179
50-AuNP-2	LP-ER	Streptavidin (protein)@AuNP	10	DNA detection by voltammetric studies	127, 180
50-AuNP-3	Two-phase method LP-ER	None, <i>n</i> -hexanethiol	Not reported	Anion-induced adsorption of Fc/AuNP hybrids on Pt electrodes	91
50-AuNP-4	LP-ER	<i>n</i> -Hexanethiol	1.8 ± 0.4	Electron and ion transport in AuNP SAMs	92
				Electrochemical studies of hybrids deposited on SAMs of mercaptoundecanoic acid (MUA) supported on ITO.	100
				Ascorbic acid sensor	94
50-AuNP-5	LP-ER	None (Au@MWCNTs)	Not determined - variable AuNP sizes	Ascorbic acid sensor	95

51-AuNP-1	LP-ER	<i>n</i> -Octanethiol	2.3 ± 0.5	Electrochemical deposition of hybrids and surface morphology studies	181						
51-AuNP-2	LP-ER	<i>n</i> -Octanethiol	2.2 ± 0.3	Electrodeposition of hybrids and lithography on a gold coated electrochemical quartz crystal balance	182, 183						
				Electrochemical studies and electrodeposition on ITO	184						
51-AuNP-3	LP-ER	<i>n</i> -Octanethiol	2.3 ± 0.5 2.9 ± 0.8 4.3 ± 1.1 6.4 ± 0.8	Electrochemical and surface studies of electrodeposited hybrids	185						
				Size influence of the electrochemical properties of deposited AuNP SAMs on ITO and surface studies	183						
				52-AuNP	LP-ER	<i>n</i> -Octanethiol	2.2 ± 0.7	Electroactive self-assembly of hybrids with AuNP at an Au(111) surface	186		
				53-AuNP	LP-ER	<i>n</i> -Octanethiol	2.2 ± 0.7	Electroactive self-assembly of hybrids with AuNP at an Au(111) surface	186		
54-AuNP	LP-ER	<i>n</i> -Octanethiol	2.6 ± 0.6	AuNP assembly on a gold surface coated with biferrocene dithiol	187						
55-AuNP	LP-ER	<i>n</i> -Octanethiol	4.5 ± 0.2	Electrochemical studies of the hybrids	188						
56-AuNP	Two-phase nanoparticle synthesis	None	2.5	Electrochemical studies of self-assembled monolayers on gold electrodes	189						
57-AuNP	LP-ER	CTAB ^b	Various sizes	Self-assembly and surface patterning	190						
58-AuNP	One-phase nanoparticle synthesis	None	1.4 ± 0.3 (M ²⁷⁺) 1.9 ± 0.3 (M ⁵⁴⁺) 3.3 ± 0.5 (M ²⁷⁺) 3.7 ± 0.5 (M ⁵⁴⁺)	Multi-redox state material	84						
						59-AuNP	LP-ER	Citrate	12.1 ± 1.2	Electrochemical sensor for detecting carbohydrate-lectin interactions	97
						60-AuNP	LP-ER	Citrate	12.1 ± 1.2	Electrochemical sensor for detecting carbohydrate-lectin interactions	97
						61-AuNP	LP-ER	<i>n</i> -Dodecanethiol	2.1	[H ₂ PO ₄] ⁻ and [ATP] ²⁻ sensors ^e	191, 192
62-AuNP	LP-ER	Citrate/ anti-human HlgG ^c	20	Electrochemical immunosensor for bovine serum albumin, alpha-lactalbumin and ovalbumin.	76						
63-AuNP^f	LP-ER	No molecular ASLs - AuNP@C-dots supported on graphene sheets	12	Ultrasensitive simultaneous detection of ascorbic acid, dopamine, uric acid and acetaminophen	58						
64-AuNP	One-phase method	TOAB ^d	5 ± 2	Phthalocyanine-coated AuNP for self-assembly on gold electrode for sensing hydrazine	71						

[a] LP-ER = ligand place-exchange reaction; [b] CTAB = cetyltrimethylammonium bromide; [c] HlgG = Human immunoglobulin G; [d] TOAB = tetra-*n*-octylammonium bromide; [e] [ATP]²⁻ = Adenosine-5'-triphosphate; [f] Corresponds to a material resulting from hybridizing the **62-AuNP** hybrids with carbon nanoclusters (CNC), graphene, and glassy carbon electrodes (GCE).

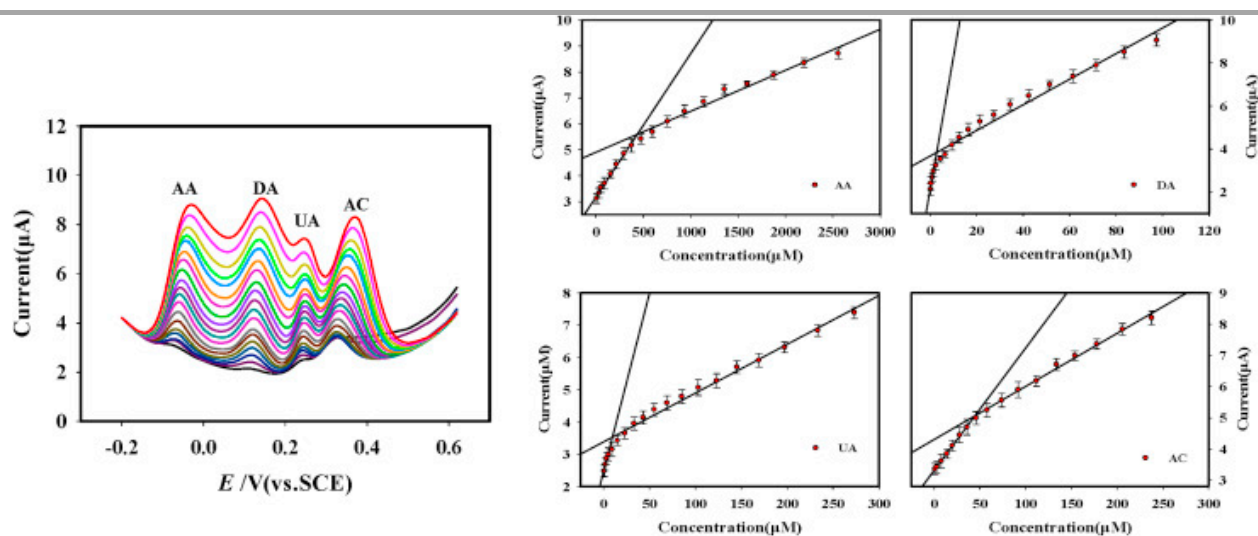


Fig. 8. Differential pulse voltammetry scans and calibration curves for the simultaneous determination of AA, DA, UA and AC using **63-AuNP** in 0.1 M PBS (pH = 7.4). Concentrations: AA (8 – 2556 μ M), DA (0.2 – 97.5 μ M), UA (0.6 – 273 μ M), AC (0.5 – 275 μ M). AA = ascorbic acid, DA = dopamine, UA = uric acid, AC = acetaminophen, PBS = phosphate-buffered saline. Reprinted with permission from ref. 58. Copyright 2016 Elsevier.

ARTICLE

The same trend is observed for the capacitance at the electrical double-layer at the core surface, a higher capacitance being found for smaller AuNP diameters; this outcome suggests that smaller AuNPs are more suitable for electrochemical devices. With this in mind, AuNP hybrids with the ω -thiohexylferrocene FSL **50** have been particularly intensively studied,^{91, 92, 94, 95, 100, 127, 179, 180} examples of applications being discussed below. Biferrocenyl/AuNP hybrids **51-AuNP-1-3**, **52-AuNP**, **53-AuNP**, **54-AuNP**, and **55-AuNP** are electrodeposited on gold and platinum electrodes at potentials positive of the second oxidation process at the biferrocenyl units. The surface morphologies of the resultant materials have been characterized,^{181, 183-185, 188, 193} similar studies have been undertaken with a ferrocenyl-coated AuNP (**56-AuNP**).¹⁸⁹ Varying the solvent when electrodepositing a poly(ferrocenyldimethylsilane)thiol/AuNP hybrid (**57-AuNP**) has a strong influence on the resultant surface-patterning and self-assembly;¹⁹⁰ pure chloroform affords AuNPs with an interparticle distance of 12 nm, whereas increasing volume fractions of cyclohexane result in aggregation of the hybrid AuNPs and an interparticle distance of 4 nm. The volume of the hybrid can also be controlled electrochemically; the poly(ferrocenyl)ated dendrimer/AuNP hybrid **58-AuNP** exhibits three reversible and stable oxidation states in solution which result in a “breathing” of the material by oxidation-state-dependent expansion and contraction of the dendrimer.⁸⁴

The attachment of ferrocene-functionalized stabilizing ligands to AuNPs has afforded sensors for the detection of species of biological importance, such as ascorbic acid (AA),^{58, 94, 95, 194} uric acid (UA),^{58, 194} acetaminophen (AC),^{58, 194} H₂PO₄⁻,^{191, 192, 195} dopamine (DA),^{58, 72, 194} DNA,^{89, 127} lectin,⁹⁷ and ATP.^{190, 191} In these systems, ferrocene is conjugated to a biological probe in order to be recognized by the specific target; the response is then recorded by electrochemical methods such as cyclic voltammetry^{127, 191} and differential pulse voltammetry.^{58, 71, 72, 76, 97} In many cases, signal amplification is effected by the presence of multiple ferrocene units at the surface of the AuNPs. Sensitivity comparable to fluorescence techniques has been achieved in the detection of DNA by electrodes consisting of ferrocene-capped streptavidin/AuNP hybrids (**50-AuNP-2**).^{89, 127} Mannosyl-substituted ferrocene/AuNP hybrids (**59-AuNP**, **60-AuNP**) have been employed in the electrochemical sensing of lectin, with detection limits three orders of magnitude better than standard colorimetric techniques.⁹⁷ A nona(silylferrocenyl) dendron/AuNP hybrid (**61-AuNP**) deposited on a platinum electrode has afforded re-usable electrodes that display selective recognition of [H₂PO₄]⁻ and [ATP]²⁻, even in the presence of other anions such as Br⁻, Cl⁻, HSO₄⁻ and NO₃⁻.^{191, 190}

More complex devices comprising multiple 1,1'-bis(1,2-dithiolane)ferrocene/AuNP hybrids (**62-AuNP**) have been used for the detection of antigens (human immunoglobulin G antigen (HlgG Ag)), dopamine, electrolytes, and drugs,⁷⁶ and a multicomponent example comprising AuNP hybrids of 1,1'-ferrocenylbis(methylene lipoic acid ester), BSA, and antibodies

supported on a carbon electrode has been used for the sensitive and selective detection of human HlgG Ag.⁷⁶ Hybridization of ferrocene-coated AuNP hybrids (**63-AuNP**) with carbon nanoclusters (CNC), graphene, and glassy carbon electrodes (GCE) has allowed simultaneous and ultrasensitive detection of AA, DA, UA and AC by differential pulse voltammetry.⁵⁸ The hybrid nanomaterial exhibits a wide dynamic range of quantification (comprising two linear ranges) for measurement of the analytes (Fig. 8). Attachment of Ni(II) phthalocyanine/AuNP hybrids (**64-AuNP**) to a gold electrode containing self-assembled monolayers of 1,6-hexanedithiol has afforded a nanostructure with high sensitivity for the detection of hydrazine (limit of detection (LOD) = 5 × 10⁻⁸ M).⁷¹

5.1.3. Electro-Optical Sensing. TMCs have played a fundamental role in the development of optoelectronic technology (e.g. cyclometallated complexes of Ir(III) in solar energy conversion, LEDs,¹⁹⁶ and light-electrochemical cells (LECs)). The electro-optical properties of Ir(III)/AuNP hybrids are of interest because AuNPs enhance the local electromagnetic field due to the LSPR. While this area remains little-explored, the photocurrent produced by a [Ru(bpy)₃]²⁺-viologen/AuNP hybrid (**65-AuNP**) deposited on a gold electrode is enhanced by one order of magnitude compared to similar electrodes lacking AuNPs (photocurrent action cross-sections at 460 nm: 4.6 $\mu\text{A mW}^{-1} \text{cm}^{-2}$ and 0.31 $\mu\text{A mW}^{-1} \text{cm}^{-2}$, respectively),⁶⁰ and electrofluorochromism studies of cyclometallated Ir(III) complexes **66** and **67** revealed modulation of the electro-optical properties on proceeding to the hybrids **66-AuNP** and **67-AuNP**;⁸¹ the hybrids display reduced electrofluorochromism and reduced potential-dependent electro-optic response compared to the free complexes **66** and **67**, respectively (Fig. 9).⁸²

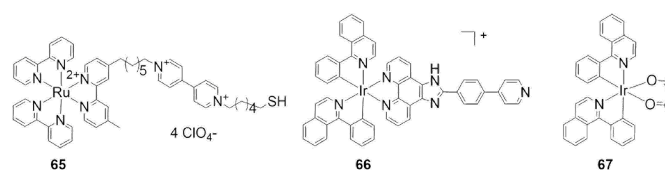


Fig. 9. Structures of complexes **65** - **67**.

5.2. Imaging

TMCs with a d⁶ electronic configuration possess interesting photophysical properties useful in imaging and microscopy.⁴¹ They can exhibit i) a large Stokes shift, which minimizes self-quenching of the signal and helps distinguish luminescence of the probe from autofluorescence, ii) long-lived excited-state lifetimes that can be beneficially exploited to remove the autofluorescence by time-gated luminescence microscopy, and

iii) excitation and emission at longer wavelengths that permit imaging with deeper tissue penetration. Additionally, the luminescence profile of complexes can be easily modified by changing the metal centre, the coordination sphere, the functional groups of the ligands and, in some cases, the oxidation state. AuNPs are electron rich materials. Their flexible surface chemistry can be exploited to attach a broad variety of chromophores that can afford enhanced spatial resolution for imaging biological environments. AuNPs can be employed in both reflective and thermal imaging. Although it is attractive to hybridize AuNPs with luminescent TMC probes in the pursuit of novel materials for imaging, the high quenching efficiencies of AuNPs towards the luminescence of the surrounding environment render it necessary to optimize the quantum yields of the TMC/AuNP hybrid materials.

The quantum yields of the complexes depend strongly on their radial distance from the AuNP core; when the metal-containing chromophore is far from the core, the quantum yield (QY) and lifetime (τ) of the fluorophore are described by the free-space condition:

$$QY = k_r / (k_r + k_{nr}) \quad (\text{Eq. 5})$$

$$\tau = 1 / (k_r + k_{nr}) \quad (\text{Eq. 6})$$

where k_r is the radiative rate and k_{nr} is the non-radiative rate. As the chromophore approaches the gold surface, the radiative and non-radiative rates increase, and the QY and τ of the hybrids are described by the following equations:

$$QY = k_r / (k_r + k_{nr} + k_{et}) \quad (\text{Eq. 7})$$

$$\tau = 1 / (k_r + k_{nr} + k_{et}) \quad (\text{Eq. 8})$$

where k_{et} is the energy and electron transfer rate attributed to the presence of the AuNP core. The immediate environment of the fluorophore does not significantly alter k_r , but strongly influences the fluorescence lifetime and intensity due to changes in k_{nr} and/or k_{et} induced by the AuNP core.

Despite the well-known luminescence quenching of AuNPs due to energy- or electron-transfer processes (k_{et}), TMC/AuNP hybrids can be engineered to display sufficiently high quantum yield to be detected by standard fluorescence microscopy techniques (Table 4). While no variation in the emission or excitation profile of the rhenium(I) tricarbonyl pyridyl complex **68** is seen on attachment to 3.1 nm AuNPs (**68-AuNP**),¹²⁹ the emission lifetime of the hybrid **68-AuNP** is shorter than the free complex **68**, and features a second component in the decay profile ($\tau = 116.8$ ns, $\tau_1 = 110$ ns, $\tau_2 = 6.8$ ns), in contrast to the mono-exponential decay observed for **68** ($\tau = 133$ ns). The Ru(II)-polypyridyl complexes (**69** - **71**) have been attached to ca. 4 nm diameter AuNPs by ligand exchange (**69-AuNP-1**, **70AuNP-1**, **71-AuNP-1**), resulting in quenching efficiencies ca. twenty times greater than those of the free complexes. The quantum yields of the red-emitting TMC/AuNP hybrids are still sufficient to image HeLa cells by confocal fluorescence microscopy in the range 600 – 700 nm, by excitation of the MLCT band of the complexes using a 488 nm laser.¹⁰⁴ The same ligands have been attached to 15 nm diameter AuNPs coated with thiol-modified DNA (**69-AuNP-2**, **70-AuNP-2**, **71-AuNP-2**) and the uptake of the hybrids into live HeLa cells monitored by fluorescence confocal microscopy imaging and TEM.¹⁰⁵

Long-chain fluorinated surfactants (FSAs, e.g. Zonyl™) attached to the AuNP surface enhance the quantum yields of Ir(III) and Ru(II) polypyridyl complexes without variation in the λ_{em} and, more importantly, avoid the luminescence quenching trade-off ordinarily associated with the AuNP core (Fig. 10).^{61, 102, 103, 131, 171, 172} For example, surface functionalization of AuNPs with the fluorinated auxiliary ligand Zonyl™ 7950® affords a three- and four-fold quantum yield enhancement in Ir/AuNP hybrids of 13 nm (**72-AuNP-1**) and 100 nm (**72-AuNP-2**) diameter, respectively.¹⁰³ The luminescence of **72** in the hybrids is less oxygen-sensitive than the free complex because the Zonyl™ FSA shields the complex from environmental oxygen. Similarly, the quantum yield of $[\text{Ru}(\text{bpy})_3]^{2+}$ (0.02) increases to 0.09 on proceeding to the hybrid $[\text{Ru}(\text{bpy})_3]^{2+}/\text{AuNP}$ by using Zonyl™ FSA and fine-tuning the radial distance of the complex.¹⁰² The luminescence properties of the hybrids do not change when varying AuNP diameters over the range 10 – 100 nm,^{59, 61, 102, 131} but are strongly dependent on the length of the spacer between the metal complex and the anchoring group, and this radial distance of the complex relative to the AuNP surface can be optimized: for example, the quantum yield of $[\text{Ru}(\text{bpy})_3]^{2+}$ is 0.02 when the complex is located ca. 0.7 nm from the AuNP surface (C_2 spacer), but three- and five-fold enhancements in the QY are observed when the distance is increased to 1.6 nm (C_6 spacer) and 2.5 nm (C_{12} spacer), respectively.¹⁰²

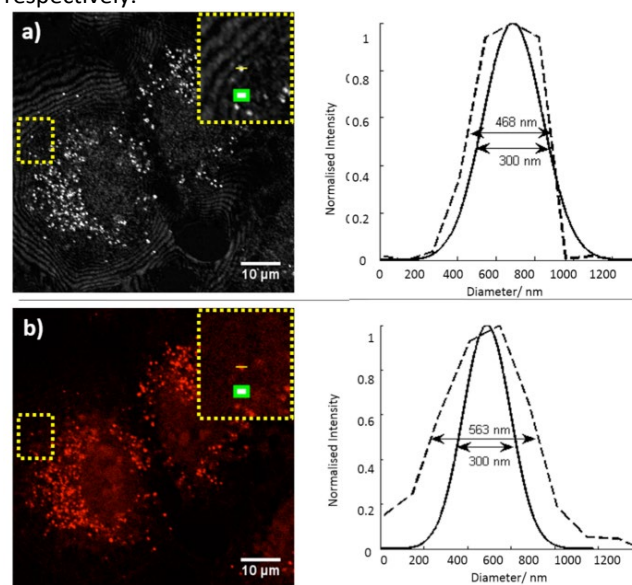


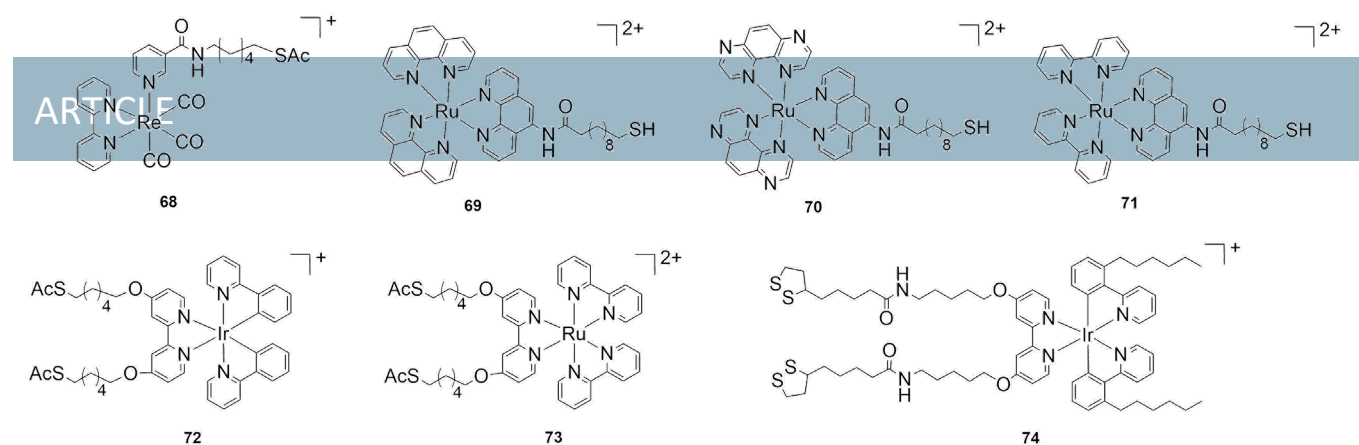
Fig 10. Reflection (a) and luminescence (b) confocal images of **73-AuNP-2** in A549 cells with their respective intensity profiles displayed in the right-hand images. Reproduced with permission from ref. 131. Copyright 2014, The Royal Society of Chemistry.

The functionalized $[\text{Ru}(\text{bpy})_3]^{2+}$ complex **73** has been deprotected in situ to give the corresponding dithiol, which was then anchored to AuNPs of 13 and 100 nm diameter, enabling dual imaging of the hybrids in a cellular environment.¹³¹ The luminescence properties of the hybrids **73-AuNP-1** and **73-AuNP-2** are independent of the size of the AuNP, and the resolution with the 100 nm core diameter hybrids is sufficient to permit single-particle imaging via confocal microscopy. The

core has been imaged by reflection microscopy ($\lambda_{\text{ex}} = 488 \text{ nm}$, $\lambda_{\text{em}} = 478 - 498 \text{ nm}$) and the Ru(II) complex imaged by fluorescence ($\lambda_{\text{ex}} = 453 \text{ nm}$, $\lambda_{\text{em}} = 555 - 800 \text{ nm}$) (Figure 10). The strong luminescence of the hybrid allows the imaging of particles associated with condensed DNA material in the nucleus of A549 cells.¹³¹ An analogous hybrid comprised of functionalized $[\text{Ir}(\text{ppy})_2(\text{bpy})]^+$ (**74**) supported on 10-100 nm diameter AuNPs is a promising material for imaging microvascular blood flow;¹⁰³ the hybrid containing the complex attached to 25 nm diameter AuNPs (**74-AuNP-2**) displays strong two-photon luminescence which has been used in two-photon lifetime imaging in cells. Detection of the fluorescence signal can be performed using two channels, one channel detecting

the long lifetime of the complex (740 ns) and the other detecting the shorter component corresponding to the AuNP (450 – 590 ns).⁶¹ All examples above display low cytotoxicity in biological environments.

Metallophthalocyanines have also been successfully hybridized with AuNPs, with strong changes in their photophysical and photochemical properties; their exceptional singlet oxygen generation capability has prompted studies in photodynamic therapy (Section 5.3). Finally, functionalization of the surface of water-soluble sodium mercaptopropionate (NaMP)/AuNPs with $^{188}\text{Re}(\text{I})$ carbonyl compounds has been explored for potential application in radioisotope imaging.¹³⁴

Table 4. Synthesis, ASLs, Size Distributions, and Linear Optical and Luminescence Properties of Hybrids Incorporating FSLs **68** - **74**.

Complex	Synthesis	ASL	Size (nm)	λ_{\max} (nm) ^b	λ_{em} (nm) ^c	Φ ^d	τ (ns) ^e	Ref
68				360	549	Not reported	133	129
68-AuNP	LP-ER ^a	MPEGSH ^f	3.1 ± 0.6	375	549	Not reported	6.8 (4%), 110 (96 %)	129
69				450	610	0.054	Not reported	104
69-AuNP-1	LP-ER	Sodium citrate	4.0 ± 1.3		610	0.002	Not reported	104
69-AuNP-2	LP-ER	Thiol-modified DNA	15.3 ± 3.0	535	610	Not reported	Not reported	105
70				450	605	0.056	Not reported	104
70-AuNP-1	LP-ER	Sodium citrate	4.3 ± 1.3		605	0.002	Not reported	104
70-AuNP-2	LP-ER	Thiol-modified DNA	15.4 ± 3.3	547	605	Not reported	Not reported	105
71				450	635	0.028	Not reported	104
71-AuNP-1	LP-ER	Sodium citrate	3.2 ± 1.1		635	0.002	Not reported	104
71-AuNP-2	LP-ER	Thiol-modified DNA	15.8 ± 3.8	525	637	Not reported	Not reported	105
72				420	570	0.05	60	103, 103
72-AuNP-1	LP-ERLP-ER LP-ER	Zonyl 7950 ^g (fluorosurfactant)	13	522 (LSPR)	570 (AuNP1-2)	0.14	Not reported	103
72-AuNP-2		Zonyl 7950 ^g (fluorosurfactant)	100	567 (LSPR)		0.19	400 ns (90 %) 90 s (10 %)	
73				462	650	0.02	260	102, 131
73-AuNP-1	LP-ER	Zonyl 7950 ^g (fluorosurfactant)	13	522 (LSPR)	640	Not reported	340 (60 %) 33 (38 %) 4567 (2 %)	131
73-AuNP-2	LP-ER	Zonyl 7950 ^g (fluorosurfactant)	100	568 (LSPR)	640	Not reported	90 (10 %) 400 (90 %)	131
74				337	580	0.04	42 (6 %) 166 (45 %) 428 (49 %)	61
74-AuNP-1	LP-ER	Zonyl FSA	13	522	590	0.05	50 (5 %) 180 (48 %) 340 (47 %)	61

74-AuNP-2	LP-ER	Zonyl FSA	25	525	590	0.05	40 (5%) 160 (42%) 330 (53%)
74-AuNP-3	LP-ER	Zonyl FSA	100	558	590	Not reported	25 (3%) 140 (43%) 340 (54%)

[a] LP-ER = ligand place-exchange reaction. [b] absorption maximum; [c] emission maximum; [d] quantum yield; [e] emission lifetime. [f] MPEGSH = methoxy polyethylene glycol thiol, LSPR = localized surface plasmon resonance, **AuNP-n** is used to denote different sizes of AuNP.

5.3 Photodynamic Therapy

Photodynamic therapy (PDT) is a promising procedure in the treatment of cancer. In PDT, excitation of photosensitisers with light of a suitable wavelength (usually in the red or NIR) results in the generation of highly cytotoxic, reactive singlet oxygen.^{197, 198} Metallophthalocyanines (MPcs) and porphyrins are promising candidates in PDT.¹⁹⁹ These 18 π -electron conjugated systems possess strong absorption bands in the wavelength range 600 – 800 nm at which biological tissue displays its maximum transparency, thereby allowing deeper penetration. In addition, they have long-lived triplet excited states capable of efficiently transferring electrons or energy to adjacent species, and as a result can afford high singlet-oxygen quantum yields (Φ_{Δ}).²⁰⁰ AuNPs can enhance the charge and energy transfer processes of the surrounding environment due to an increase in the non-radiative rate, leading to a more efficient generation of singlet oxygen.²⁰¹ They have also been employed as platforms for drug delivery due to their excellent biocompatibility;²⁰² AuNPs have been functionalized with water-soluble ASLs to deliver hydrophobic drugs to specific tissue sites without modification of the molecular structure of the drug. Hybridization of MPcs with AuNPs is therefore of considerable interest, and leads to enhancement in the therapeutic performance in PDT due to i) the increase in the singlet oxygen quantum yield (Φ_{Δ}) by plasmon-enhanced light absorption of the chromophore, ii) the synergetic effect of photothermal treatment by AuNPs and singlet oxygen generated by the phthalocyanine, iii) the delivery of higher concentrations of the MPc photosensitizer to the tumour cells, and iv) improvements in the solubility of phthalocyanines in polar protic solvents and biological environments.^{62, 197} Indeed, one of the major drawbacks of MPcs (M = Al, Cu, Co, Mg, Ni, Zn) is their poor solubility in polar protic solvents, particularly water, which restricts their applications in medicine;²⁰⁰ hybridizing MPcs with AuNPs can solve this problem. For example, hybridization of the toluene-soluble thiol-tethered Zn(II) phthalocyanine **75** with TOAB/AuNPs affords **75-AuNP-1** (Table 5), which can be redispersed in ethanol.⁵⁵ A remarkable 50% enhancement in the generation of singlet oxygen is seen for the hybrid **75-AuNP-1** ($\Phi_{\Delta} = 0.65$) compared to the free complex **75** ($\Phi_{\Delta} = 0.45$),⁵⁵ an observation that lead to the introduction of different ionic functional groups such as carboxylate,⁷⁵ quaternary amines and sulfonates,⁵⁷ and non-ionic functional groups such as amines,¹⁵⁸ pyrrolidone,²⁰³ thiols,^{55, 75, 83} thioethers,^{57, 73, 75, 79, 204} and disulfides²⁰⁵ at the

MPc to facilitate interaction with the AuNP surface, with the expectation of improving the overall solubility of the hybrid in biological environments. However, aggregation of the AuNPs can occur due to the resulting close-packing of the Pcs on the AuNP surface, and in these cases surfactants such as Triton™ X-100 have been employed to preserve the colloidal stability of the hybrids.⁷³

Most MPc/AuNP hybrids exhibit greater triplet as well as singlet oxygen quantum yields than the analogous free complexes; the decreases in luminescence quantum yields and increases in triplet excited-state lifetimes arise from the strong interactions of the MPcs with the AuNP cores, and this correlates strongly with increased generation of singlet oxygen.

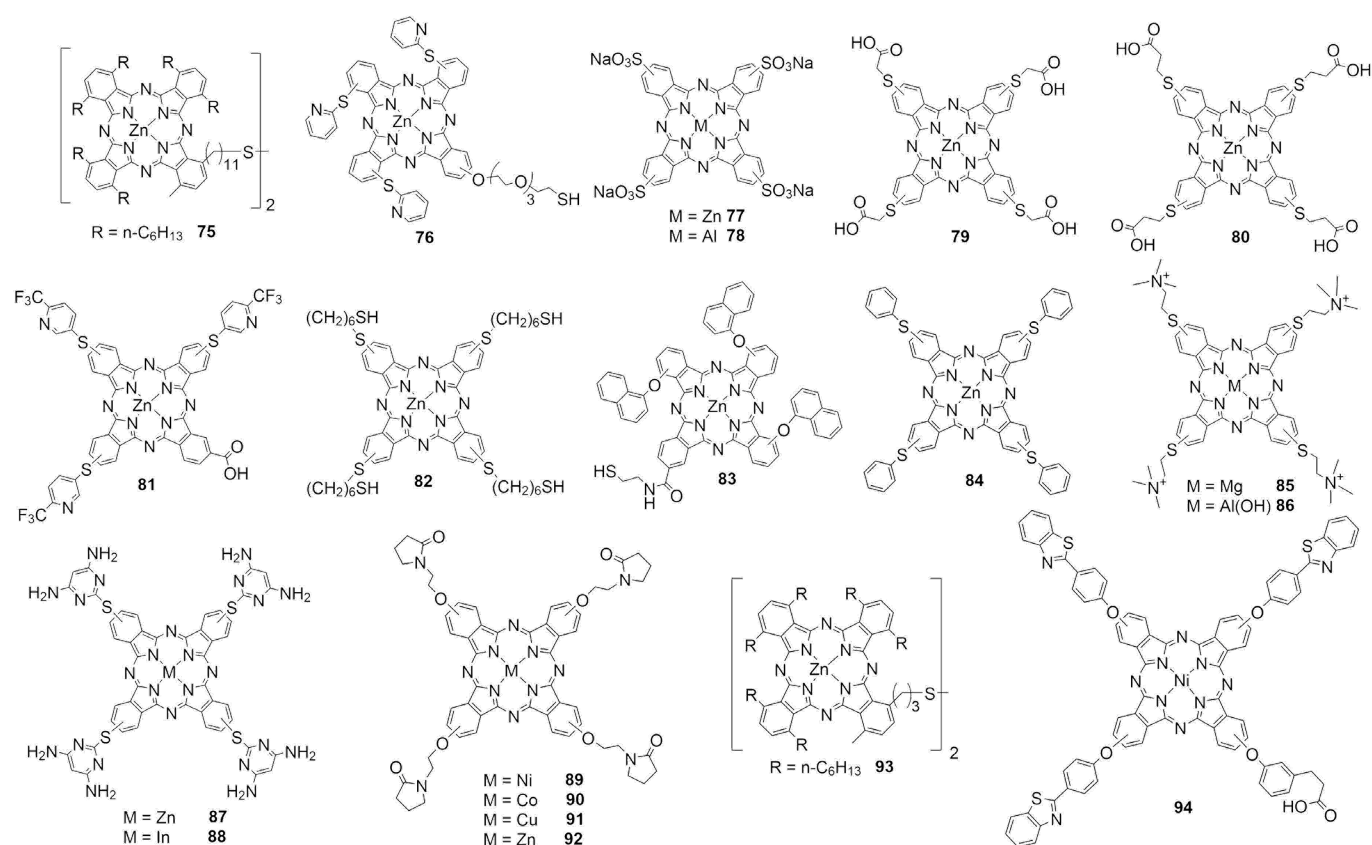
The shape of the AuNPs has a key effect on the progress of the LP-ER; while the CTAC (CTAC = cetyltrimethylammonium chloride) ASLs are displaced with aggregation of AuNP stars, the spherical AuNP analogues undergo LP-ER with MPcs to afford stable hybrids. The spherical hybrid **79-AuNP** prepared by this procedure displays an 11-fold increase in its quantum yield compared to that of the free sensitizer.⁵⁷ Varying the number of linking units, the radial distance of the complex with respect to the AuNPs, the type of anchoring group, and the metal centre have all been explored, in efforts to maximize the Φ_{τ} and Φ_{Δ} values; as expected, proximity of the MPcs to the AuNP surface results in strong quenching and a decrease in luminescence quantum yield, together with an increase in singlet oxygen generation. Quenching in MPc/AuNP hybrids results from exciton-plasmon interactions following aggregation of the phthalocyanines on the surface of the AuNP.²⁰⁶ Mie theory suggests that the maximum absorption enhancement is expected at an AuNP diameter of ca. 80 nm, with an enhancement factor of 5.3 compared to the free complex assembled as a monolayer on a gold surface. Studies to assess the influence of the anchoring groups have shown that, for a series of AuNP hybrids with phthalocyanines bearing a carboxylic acid (**81**), four thioether units (**82**) or one thiol group (**83**), the highest enhancement in Φ_{τ} is observed for the thiol-tethered phthalocyanine/AuNP hybrid **83-AuNP**, from 0.63 for the free complex **83** to 0.71 for **83-AuNP**;⁷⁵ mild fluorescence quenching is observed for the tetra-(thioether) MPc-functionalized **84-AuNP**.⁷⁹ Tethering via ionic functional groups, such as quaternary ammonium salts, results in an increase of ca. 15% in Φ_{τ} when the Mg^{2+} (**85**) or $[\text{Al}(\text{OH})]^{2+}$ (**86**) phthalocyanines are hybridized with 5.4 nm diameter AuNPs (**85-AuNP**, **86-AuNP**).⁷³ Comparison of AuNPs, gold-coated iron oxide nanoparticles ($\text{Au}@\text{Fe}_3\text{O}_4$), and quantum dots (QDs) hybridized with zinc(II) (**87**) or indium(III) (**88**) MPcs¹⁵⁸ shows the highest

Φ_{Δ} values for the AuNP hybrids (e.g. **88-AuNP** Φ_{Δ} = 0.92 c.f. **88-Au@Fe₃O₄** Φ_{Δ} = 0.46 and **88-QDs** Φ_{Δ} = 0.34). Compared to the free MPCs, the MPC/AuNP hybrids (M = Co²⁺ (**90**), Cu²⁺ (**91**)) exhibit almost double the length of the lifetimes, whereas the nickel- and zinc-containing hybrids **89-AuNP** and **92-AuNP** show similar lifetimes to the free complex **92**.²⁰³

Zn(II)Pc/AuNP hybrids slow tumour growth of amelanotic melanoma following *in vivo* PDT, and with a lower persistence of the hybrid than the free MPC in the tissue.²⁰⁵ Related studies have further defined their potential in PDT. Hybrids of Zn(II)Pc **75** and AuNPs that are stabilized with cellulose, lactose, TOAB, or molecules of biological importance such as antibodies, lectins, carbohydrates, peptides, aptamers, and folic and hyaluronic acids possess good solubility in biological environments and function as recognition sites for targeting certain types of cancer.⁶² Indeed, the hybrids **75-AuNP-1-3** and

93-AuNP are effective in the treatment of amelanotic melanoma, breast cancer and colon adenocarcinoma.⁶² The hybrids function in two ways: the AuNP enhances the performance of the photosensitiser (the MPC) in PDT, and the hybrids exhibit negligible dark cytotoxicity and efficient cytotoxicity when excited at 633 nm. Similar observations were reported for Ni(II)Pc/citrate-capped/AuNP hybrids **94-AuNP-1**. Chitosan has also been incorporated (**94-AuNP-2**) to improve TMC/AuNP hybrid delivery to the biological environment.⁷⁴ However, while outstanding anti-tumor activity has been observed in MPC/AuNP hybrids, the mobility of hybrids at the biological site is greatly reduced, in contrast to free MPCs which diffuse readily in biological environments.⁶² Greater control over the duration of the drug/host interaction is needed for implementation of these hybrid nanomaterials in biological systems.

Table 5. Synthesis, ASLs, Size Distributions, and Linear Optical and Luminescence Properties of Hybrids Incorporating FSLs **75 - 94**.



Complex	Synthesis	ASL	Size (nm)	λ_{\max}^e	λ_{em}^f	Φ_f^g	Φ_T^h	τ (ns) ⁱ	Φ_{Δ}^j	Ref.
75				705	715	Not reported	Not reported	2.1 (91 %) 1.11 (9 %)	0.45	55, 123, 205
75-AuNP-1	Two-phase method	TOAB ^b	2 – 4 nm	695	715	Not reported	Not reported	1.8 (98 %) 3.6 (2 %)	0.65	55, 124, 126, 205
75-AuNP-2	One-phase method	^c (3000 Da)	3.83 ± 0.99	705	660 – 850	0.0020	Not reported	Not reported	Not reported	123
75-AuNP-3	One-phase method	^c (3247 Da)	4.5 ± 1.3	705	Not reported	Not reported	Not reported	Not reported	Not reported	124

ARTICLE											Journal Name
76				694	708	0.06	0.63	217 000 (τ_T)	045	83	
76-AuNP	LP-ER ^a	TOAB	5.5	692	706	0.04	0.84	455 000 (τ_T)	068	83	
77	-	-	-	666	682	0.13	Not reported	2.7 (93 %) 0.7 (7%)	Not reported	57	
77-AuNP	LP-ER	TOAB	20	668	682	0.08	Not reported	2.7 (90 %) 0.7 (10 %)	Not reported	57	
78				675	682	0.50	Not reported	5.0	Not reported	57	
78-AuNP	LP-ER	TOAB	20	677	692	0.67	Not reported	5.0 (98 %) 1.3 (2 %)	Not reported	57	
79				683	709	0.03	Not reported	3.1 (33 %) 1.8 (34 %) 0.4 (33 %)	Not reported	57	
79-AuNP	LP-ER	TOAB	20	687	707	0.34	Not reported	3.0 (74 %) 1.9 (26 %)	Not reported	57	
80				643	Not reported	0.11	Not reported	5.25 (19 %) 2.96 (81 %)	Not reported	57	
80-AuNP	LP-ER	TOAB	20	647	708	0.36	Not reported	Not reported	Not reported	57	
81				667, 703	708	0.04	0.68	110 000	Not reported	75	
81-AuNP	LLP-ER	TOAB	5.97 – 7.87	667, 704	709	0.02	0.71	92 000 (τ_T)	Not reported	75	
82				704	716	0.15	0.75	304 000 (τ_T)	Not reported	75	
82-AuNP-1	LP-ER	TOAB	5.97 – 7.87	698	706	0.07	0.69	87 000 (τ_T)	Not reported	75	
82-AuNP-2	LP-ER	TOAB	5.96	697	706	0.07	0.80	84 000 (τ_T)	0.74	204	
83				692	704	0.05	0.63	140 000 (τ_T)	Not reported	75	
83-AuNP	LP-ER	TOAB	5.97 – 7.87	689	701	0.04	0.71	70 000	Not reported	75	
84				692	702	0.15	Not reported	2.60	Not reported	79	
84-AuNP	LP-ER	TOAB	5 (AFM)	685	698	0.09	Not reported	4.23 (73 %) 1.74 (27 %)	Not reported	79	
85				687	699	0.16	0.29	720 000 (τ_T)	Not reported	73	
85-AuNP	LP-ER	Citrate	5.4 (by XRD)	687	699	0.10	0.35	420 000 (τ_T)	Not reported	73	
86				691	703	0.11	0.46	487 000 (τ_T)		73	
86-AuNP	LP-ER	Citrate	-5.4 (by XRD)	691	703	0.07	0.54	380 000 (τ_T)	Not reported	73	
87				689	705	0.11	0.83	351 000 (τ_T)	0.30	158	
87-AuNP	LP-ER	Hexadecylani line	7.48	689	705	0.03	0.84	244 000 (τ_T)	0.47	158	
88				704	705	0.01	0.88	57 000 (τ_T)	0.33	158	
88-AuNP	LP-ER	Hexadecylani line	7.64	700	705	<0.01	0.92	107 000 (τ_T)	0.52	158	
89				672	715	0.03	Not reported	5.42	Not reported	203	
89-AuNP	LP-ER	MPEG ^d	14.9 nm	673	708	0.02	Not reported	5.94	Not reported	203	
90				668	723	0.02	Not reported	3.33	Not reported	203	
90-AuNP	LP-ER	MPEG	14.9 nm	674	The hybrid was not luminescent	Not reported	Not reported	6.02	Not reported	203	
91				679	724	0.02	Not reported	3.63	Not reported	203	
91-AuNP	LP-ER	MPEG	14.9 nm	681	682	0.008	Not reported	5.52	Not reported	203	
92				678	690	0.07	Not reported	3.65	Not reported	203	
92-AuNP	LP-ER	MPEG	14.9 nm	679	696	0.05	Not reported	2.88	Not reported	203	
93				698	660 - 850	0.026	Not reported	Not reported	Not reported	123	
93-AuNP	One-phase method	^c (3000 Da)	3.41 ± 1.16	705	660 - 850	0.0042	Not reported	Not reported	Not reported	123	
94				680	698	0.15	0.73	238 000 (τ_T)	0.69	74	
94-AuNP-1	LP-ER	Citrate	13.4 (DLS)	680	698	0.11	0.89	227 000 (τ_T)	0.80	74	
94-AuNP-2	LP-ER	Chitosan	329 (DLS)	679	698	0.12	0.81	231 000 (τ_T)	0.75	74	

[a] LP-ER = ligand place-exchange reaction; [b] TOAB = tetra-*n*-octylammonium bromide; [c] α -thio- ω -carboxy polyethylene glycol; [d] a thiolated methoxypolyethylene glycol, MW = 2000; [e] absorption maximum; [f] emission maximum; [g] fluorescence quantum yield; [h] triplet quantum yield; [i] emission lifetime, τ_T specifies the triplet excited state lifetime; [j] singlet oxygen generation quantum yield.

5.4. Nonlinear Optics

The NLO and particularly nonlinear absorption (NLA) properties of molecular and nano-materials are of great interest because of their potential applications in medicine, 3D patterning, optical data storage, optical limiting (OL) and telecommunications.^{43, 207-209} AuNPs exhibit NLA in processes including saturable absorption (SA), two-photon absorption (2PA), excited-state absorption (ESA), and two-photon excited fluorescence (2PEF) because of highly polarizable valence band electrons at the AuNP surface,^{210, 211} and they can enhance the NLO response of the surrounding environment by coupling the incident electromagnetic radiation with LSPR.¹⁴ AuNPs have responses on the femtosecond to nanosecond timescale, which is attractive for ultrafast applications such as OL devices for eye and optical sensor protection. However, bare AuNPs or weakly-stabilized AuNPs often precipitate or suffer structural modifications under the intense laser radiation required to observe NLO phenomena,²¹² so effective passivation of AuNPs is a necessary step to exploiting their potential.

TMCs exhibit intense MLCT and LMCT transitions that arise from the strong $d\pi$ - $\pi\pi$ orbital overlap between the metal centre and the ligand; as a result, they are of significant current interest in applications such as 2PA imaging and OL.²¹³ The redox reversibility exhibited by certain TMCs can be exploited to introduce electrochemically-triggered NLA switching which permits greater control of the optical properties of molecular materials.²¹⁴ Various studies have shown that TMCs display much larger NLA activity than their organic counterparts; this is particularly the case for metallated porphyrins and mono- and bis-alkynyl complexes of the late transition metals.^{44, 215-217}

The LSPR of AuNPs behaves as a strong dipole when it interacts with the electric component of the incident electromagnetic field, and thus the NLA responses of TMC/AuNP hybrids can be enhanced at the surface of the AuNP (Table 6). Hybridization of the Ir(III) complex **74** and AuNPs results in a 53-fold enhancement of σ_2 at 760 nm compared to the free complex (**74** 38 GM cf **74-AuNP2** 2000 GM), the enormous increase being attributed to the LSPR of the AuNP core.⁶¹ A blend of gold nanoparticles and the tetra-substituted ZnPc **95** in THF solution shows NLA due to self-healing of the AuNPs (**95-AuNP**),²¹² attributed to AuNP aggregation and surface passivation induced by **95** after melting of the AuNPs. The blend displays better OL performance than the AuNP or the ZnPc alone, and indeed has better OL performance than a fullerene benchmark with similar linear transmittance to 9 ns pulsed laser radiation at 532 nm (note that bare AuNPs precipitate under the same experimental conditions). The

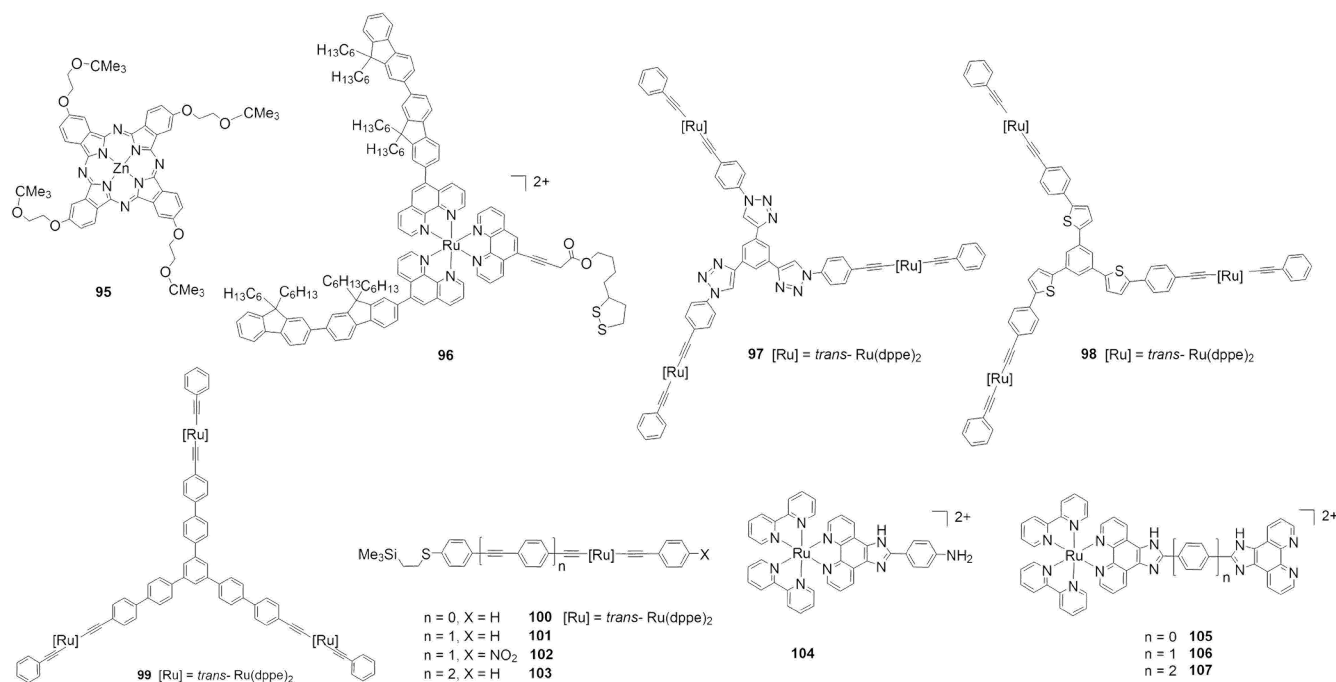
tris(1,10-phenanthroline)ruthenium(II) complex **96** exhibits NLA at short wavelengths (550 – 600 nm, assessed via the Z-scan technique and a 130 fs pulsed tunable laser), while the hybrid **96-AuNP** (resulting from its attachment to 2 – 3 nm diameter AuNPs) is a saturable absorber in the same wavelength range;^{218, 219} these TMC/AuNP hybrids are possible sensitizers in two-photon PDT.²¹⁹

Exceptional 2PA performance is seen in metal alkynyl-based stars **97** - **99** attached to AuNPs of sizes ranging from 2.5 to 4.6 nm, with the highest 2PA cross-section of 3,000,000 GM at 500 nm (using 130 fs pulses) being observed for **98-AuNP**.⁵⁶ The organoruthenium/AuNP hybrids are highly transparent in the vis-NIR region, and exhibit better NLA performance at longer wavelengths than purely organic hybrids of a similar size (e.g. **98-AuNP** $\sigma_{2,750} = 46,000 \pm 8100$ GM, **99-AuNP** $\sigma_{2,800} = 130,000 \pm 32,000$ GM c.f. *n*-dodecanethiol-coated AuNP $\sigma_{2,750} = 23,000 \pm 4300$ GM). AuNP hybrids of the organoruthenium OPEs **100**, **101**, **102**, and **103**, which possess different length arylalkynyl spacers, display strong 2PA activity in the UV-vis region and unprecedented 2PA performance in the second biological window (**101-AuNP** $\sigma_{2,1050} = 20,000 \pm 10,000$ GM, **102-AuNP** $\sigma_{2,1050} = 26,000 \pm 4000$ GM, **103-AuNP** $\sigma_{2,1050} = 38,000 \pm 13,000$ GM). Again, the organometallic/AuNP hybrids show superior performance to their organic counterpart, for which weak NLA activity is seen at wavelengths beyond 800 nm ($\sigma_{2,1050} = 540 \pm 130$ GM).¹⁶⁴

Ru(II) complex/AuNP hybrids have been used for sensing thiol-containing amino acids such as glutathione (GSH), homocysteine (Hcy) and cysteine (Cys) by exploiting changes in NLO properties. The thiol species displace complex **104** from the surface of the hybrid **104-AuNP**, thereby recovering the 2PEF activity of the AuNP and the σ_2 profile of the complex (**104** $\sigma_2 = 350$ GM at 800 nm). This permits detection of the analytes with high sensitivity (LOD of 2.15×10^{-8} M (GSH), 4.86×10^{-8} M (Hcy), 4.86×10^{-8} M (Cys)) and over a wide range of concentrations (from 10^{-8} – 10^{-5} M).⁷⁰

Hybrids of the ruthenium(II) polypyridyl complexes **105-107** and 42 to 47 nm diameter AuNPs exhibit 2PEF (**105-AuNP** $n = 0$, $\sigma_2 = 7.8$ GM; **106-AuNP** $n = 1$, $\sigma_2 = 187$ GM; **107-AuNP** $n = 2$, $\sigma_{2,808} = 105$ GM) and high photothermal therapy efficiency (η) in living cells (**105-AuNP** $\eta = 25.9$ %; **106-AuNP** $\eta = 33.3$ %; **107-AuNP** $\eta = 23.5$ %).⁸⁰ Photothermal images of the hybrids at equal concentrations (Fig. 11a) reveal that **106-AuNP** reaches ca. 60 °C in ca. 5 mins (this is the highest temperature from the series) upon excitation with an 808 nm laser with an intensity power of 0.8 W cm^{-2} (Fig. 11b). Cell viability studies on HeLa cancer cell cultures indicate that **106-AuNP** is not cytotoxic when not irradiated (Fig. 11c), but irradiation at 808 nm with power intensities ranging from 0.3 – 1.0 mW cm^{-2} induces cell

death of more than 80 % of the culture; in contrast, the free complex **106** displays poor activity (Fig. 11d), suggesting that this hybrid could be a promising anti-cancer agent in photothermal therapy, and a luminescent probe in 2PEF imaging.

Table 6. Synthesis, Size Distributions, Linear Optical, and Nonlinear Optical Properties of Hybrids Incorporating FSLs **76, 95 - 107**.

Complex	Synthesis	Size (nm)	λ_{max}^a	λ_{em}^b	λ_{ex}^c	Φ^d	σ_2 (λ_{max}) ^e	Ref.
74			377	580	375	0.04	38 (760)	61
74-AuNP2	Not reported	22 ± 6	525	590	375	0.05	2000 (760)	61
95			677	Not reported	Not reported	Not reported	Not reported	212
95-AuNP	Coulombic interactions	23	677	Not reported	Not reported	Not reported	645 mJ/cm ² f	212
96			410-460 (plateau)	619	440	0.030	7000 (600)	218
96-AuNP	Two-phase method	2-3	410-460 (plateau)	619	440	0.001	384,000 (675)	218
97			368	Not reported	Not reported	Not reported	650 ± 160 (750)	37
97-AuNP	Two-phase method	2.7 ± 0.7	530	500	440	10 ⁻⁶	4000 ± 700 (750)	56
98			428	Not reported	Not reported	Not reported	3500 ± 580 (530)	56
98-AuNP	Two-phase method	2.7 ± 0.5	535	550	476	10 ⁻⁴	3.0 × 10 ⁶ ± 7.3 × 10 ⁵ (500)	56
99			384	Not reported	Not reported	Not reported	Not reported	56
99-AuNP	Two-phase method	4.6 ± 1.6	550	500	451	10 ⁻⁶	130,000 ± 32 000 (800)	56
100			335	Not reported	Not reported	Not reported	60 ± 10 (640)	164
100-AuNP	Two-phase method	2.5 ± 0.6	523 (LSPR)	Not reported	Not reported	Not reported	104,000 ± 18 000 (625)	164
101			389	418	340	0.023	250 ± 20 (800)	164
101-AuNP	Two-phase method	2.3 ± 0.7	526 (LSPR)	423	340	0.008	190,000 ± 12,000 (775)	164
102			460	406	340	0.007	760 ± 50 (760)	164
102-AuNP	Two-phase method	1.8 ± 0.7	Not reported	366	340	10 ⁻⁶	170,000 ± 33,000 (625)	164
103			413	412	340	0.044	520 ± 90 (780)	164
103-AuNP	Two-phase method	2.3 ± 0.6	Not reported	393	340	0.023	232,000 ± 39 000 (600)	164
104			458	615	458	Not reported	350 (800)	70
104-AuNP	Two-phase method	4 - 11	580	615	458	Not reported	25 (800)	70
105			458	~ 610	460	Not reported	215 (808)	80
105-AuNP	Two-phase method	42.0 ± 2.0	570	~ 610	460	Not reported	7.8 (808)	80
106			459	~ 620	460	Not reported	394 (808)	80, 221
106-AuNP	Two-phase method	45 ± 1.5	570	~ 620	460	Not reported	187 (808)	80
107			458	~ 620	460	Not reported	176 (808)	80
107-AuNP	Two-phase method	47 ± 2.0	590	~ 620	460	Not reported	105 (808)	80

[a] Absorption maximum; [b] emission maximum; [c] excitation wavelength; [d] fluorescence quantum yield; [e] σ_2 values in GM (1 GM = 10⁻⁵⁰ cm⁴ s photon⁻¹); [f] optical limiting threshold value with 85 - 99 % transmittance using 532 nm laser (9 ns).

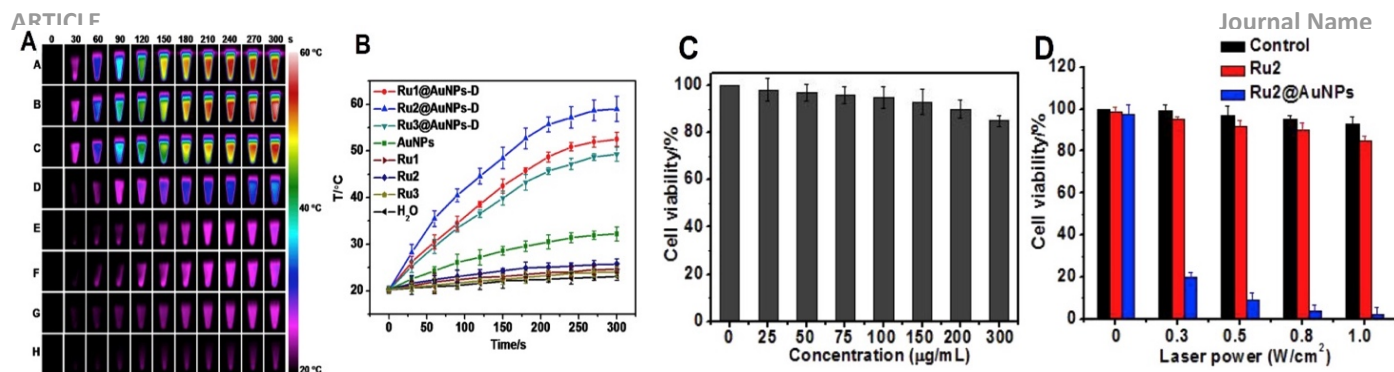


Fig 11. A) Photothermal images of **106-AuNP** and B) plot of the temperature versus the irradiation time. Cancer cell viability plots before (C) and after (D) photothermal therapy (left to right). Reproduced with permission from ref. 80. Copyright 2015 Elsevier.

5.5. Catalysis

AuNPs possess a high surface energy and a high surface-to-volume ratio, and have consequently been explored as catalysts for a broad variety of organic reactions (e.g. nucleophilic additions, hydrogenation,²²⁰ oxidative coupling, carbon-carbon coupling, etc.).^{23, 25, 222} TMCs are fundamental to organic synthesis, and have been applied inter alia in various carbon-carbon and heteroatom-carbon cross-coupling reactions and hydrogenation reactions. Compared to individual AuNPs or TMCs, TMC/AuNP hybrids have been considerably less explored as catalysts; early studies have been reviewed elsewhere.^{119, 223} Since these earlier reviews, polyferrocenylated/AuNP hybrids have been examined as catalysts for the reduction of *p*-nitrophenol, and shown to exhibit considerably higher activity than organic thiol-capped AuNPs,^{63, 64} while hybrids of RuHCl(CO)(PPh₃)₃ and AuNPs coated with thiolated branched 1,3,5-triazines have been assessed as catalysts in Suzuki-Miyaura cross-coupling; although conversions of up to 85 % were noted,⁹⁶ the AuNPs did not provide any enhancement of activity compared to the TMC.

Conclusions and Future Prospects

The hybridization of molecular materials with AuNPs is of continuing interest to the scientific community due to the potential enhancements in chemical and physical properties that can ensue. Although hybridization of AuNPs with organics has thus far dominated this field, as summarized above the hybridization of AuNPs with TMCs has been shown to afford nanomaterials with enhanced properties that are of interest in applications such as photodynamic therapy, nonlinear optics, imaging and sensors.

This exciting contemporary field is simultaneously affording significant challenges and opportunities. The hybridization of disparate materials (in the present case transition metal complexes from the field of molecular chemistry and AuNPs from the nanoparticle domain), with their distinct synthetic procedures and physical properties, poses challenges in synthesis and characterization because the synthetic

procedures and characterization techniques usually deployed for the TMC or AuNP in isolation may not be appropriate for the hybrid material. As a consequence of these difficulties, the majority of the TMCs to have been exploited thus far in AuNP hybrid syntheses have been robust “classical” examples that have straightforward syntheses and well-defined properties (e.g. porphyrins and ruthenium(II) tris-bipyridyl derivatives from coordination chemistry, ferrocene derivatives and metal alkynyls from organometallic chemistry). We can confidently anticipate that, as familiarity increases in handling the unique synthesis/characterization requirements of these hybrid materials, the broad palette of extant TMCs will be exploited in the search for new and enhanced properties. Simultaneously, the hybridization of TMCs with gold nano-crystals with shapes other than spherical or pseudo-spherical (e.g. nano-rods, nano-triangles, nano-plates, nano-cubes, etc.) is expected to increase, because hybridization with non-spherical nanoobjects will extend the capabilities of hybrids (for example, providing field enhancement at longer wavelengths, and thereby potentially affording access to materials functioning in the biological or telecommunications windows; as one possibility, the two LSPR modes present in gold nanorods can enhance the optical properties of TMCs displaying absorption in the visible and/or NIR (e.g. MPCs, porphyrins), and this is beneficial for applications in photothermal therapy, imaging and nonlinear optics^{56, 61, 62}). The hybridization of TMCs with AuNPs that is the focus of this review is, in a sense, a microcosm of a wider trend in chemistry; viewed more broadly, the hybridization of TMCs with nanomaterials is opening new vistas at the nexus of coordination chemistry/organometallic chemistry and nanoscience, and exciting new developments in this frontier area can be confidently anticipated.

As has been highlighted in this review, the strong enhancement in singlet oxygen generation of MPC/AuNP hybrids compared to that of the individual components promises novel anti-cancer drugs, assuming that other necessary aspects of PDT performance (biocompatibility, bi-mobility) are addressed. The simultaneous photo- and thermal-therapy from the combination of MPCs and AuNPs is also an

excellent example of the multifunctionality that is possible with hybrids. Other multifunctional TMC/AuNP hybrids have been exploited for multimodal imaging, while hybridization to afford novel theranostic materials also has considerable potential.

TMC/AuNP hybrids have been shown to be efficient electrochemical sensors and a critical component in multicomponent devices for the recognition of species of biological importance with exceptional sensitivity. The incorporation of TMC chromophores with reversible redox events into hybrids is also expected to enhance optical switching, with applications as advanced photonic materials. Examples of TMC/AuNPs suitable for electro-optical sensors and NLO devices remain scarce, but recent progress has demonstrated their promise in NLA applications. TMC/AuNP hybrids may also be suitable for applications in energy storage and energy conversion (e.g. redox flow batteries, solar cells), but if the redox processes occur in solution, challenges remain in the careful design of the shell of the hybrids, so as to avoid aggregation of the AuNP cores.

Finally, as mentioned above, while most of the “classic” TMCs have been hybridized with AuNPs and there remain many potential TMC candidates yet to be explored, a more crucial need is for quantitative structure-property studies to allow a detailed understanding of distance dependencies and associated quenching; in most reports so far, such studies remain to be promulgated.

Conflicts of interest

There are no conflicts to declare.

Acknowledgements

We thank the Australian Research Council for support of this work (grant no. DP170100408). C.Q. thanks Becas Chile (CONICYT) for financial support in the form of a PhD scholarship.

Notes and references

- M. Wright and A. Uddin, *Solar Energy Mater. Solar Cells*, 2012, **107**, 87-111.
- R. Liu, *Materials*, 2014, **7**, 2747-2771.
- P. Reiss, E. Couderc, J. De Girolamo and A. Pron, *Nanoscale*, 2011, **3**, 446-489.
- D. P. Dubal, O. Ayyad, V. Ruiz and P. Gomez-Romero, *Chem. Soc. Rev.*, 2015, **44**, 1777-1790.
- U. Diaz, D. Brunel and A. Corma, *Chem. Soc. Rev.*, 2013, **42**, 4083-4097.
- M. B. Gawande, Y. Monga, R. Zboril and R. K. Sharma, *Coord. Chem. Rev.*, 2015, **288**, 118-143.
- S. Wang, Y. Kang, L. Wang, H. Zhang, Y. Wang and Y. Wang, *Sens. Actuator B-Chem.*, 2013, **182**, 467-481.
- P. Gomez-Romero, *Adv. Mater.*, 2001, **13**, 163-174.
- M. S. Saveleva, K. Eftekhari, A. Abalymov, T. E. L. Douglas, D. Volodkin, B. V. Parakhonskiy and A. G. Skirtach, *Front. Chem.*, 2019, **7**, 179-200.
- M. Srinivasan, M. Rajabi and S. A. Mousa, *Nanomaterials*, 2015, **5**, 1690-1703.
- J. Feng and H. Zhang, *Chem. Soc. Rev.*, 2013, **42**, 387-410.
- K. Saha, S. S. Agasti, C. Kim, X. Li and V. M. Rotello, *Chem. Rev.*, 2012, **112**, 2739-2779.
- P. K. Jain, X. Huang, I. H. El-Sayed and M. A. El-Sayed, *Acc. Chem. Res.*, 2008, **41**, 1578-1586.
- M. Kauranen and A. V. Zayats, *Nat. Photon.*, 2012, **6**, 737-748.
- M. Notarianni, K. Vernon, A. Chou, M. Aljada, J. Liu and N. Motta, *Sol. Energy*, 2014, **106**, 23-37.
- S. Pillai and M. A. Green, *Sol. Energy Mater. Sol. Cells*, 2010, **94**, 1481-1486.
- S. S. Lucky, K. C. Soo and Y. Zhang, *Chem. Rev.*, 2015, **115**, 1990-2042.
- D. A. Giljohann, D. S. Seferos, W. L. Daniel, M. D. Massich, P. C. Patel and C. A. Mirkin, *Angew. Chem. Int. Ed.*, 2010, **49**, 3280-3294.
- S. Eustis and M. A. El-Sayed, *Chem. Soc. Rev.*, 2006, **35**, 209-217.
- X. Huang and M. A. El-Sayed, *J. Adv. Res.*, 2010, **1**, 13-28.
- E. Boisselier and D. Astruc, *Chem. Soc. Rev.*, 2009, **38**, 1759-1782.
- Y.-C. Yeh, B. Creran and V. M. Rotello, *Nanoscale*, 2012, **4**, 1871-1880.
- A. Corma and H. Garcia, *Chem. Soc. Rev.*, 2008, **37**, 2096-2126.
- M. C. Daniel and D. Astruc, *Chem. Rev.*, 2004, **104**, 293-346.
- Y. Zhang, X. Cui, F. Shi and Y. Deng, *Chem. Rev.*, 2012, **112**, 2467-2505.
- E. Roduner, *Chem. Soc. Rev.*, 2006, **35**, 583-592.
- R. Herizchi, E. Abbasi, M. Milani and A. Akbarzadeh, *Artif. Cells Nanomed. Biotechnol.*, 2016, **44**, 596-602.
- P. Zhao, N. Li and D. Astruc, *Coord. Chem. Rev.*, 2013, **257**, 638-665.
- A. J. Mieszawska, W. J. Mulder, Z. A. Fayad and D. P. Cormode, *Mol. Pharm.*, 2013, **10**, 831-847.
- C. M. Cobley, J. Chen, E. C. Cho, L. V. Wang and Y. Xia, *Chem. Soc. Rev.*, 2011, **40**, 44-56.
- A. N. Shipway, E. Katz and I. Willner, *ChemPhysChem*, 2000, **1**, 18-52.
- D. H. Wang, D. Y. Kim, K. W. Choi, J. H. Seo, S. H. Im, J. H. Park, O. O. Park and A. J. Heeger, *Angew. Chem. Int. Ed.*, 2011, **50**, 5519-5523.
- H. Jans and Q. Huo, *Chem. Soc. Rev.*, 2012, **41**, 2849-2866.
- U. Resch-Genger, M. Grabolle, S. Cavaliere-Jaricot, R. Nitschke and T. Nann, *Nat. Methods*, 2008, **5**, 763-775.
- C. Eggeling, J. Widengren, R. Rigler and C. A. Seidel, *Anal. Chem.*, 1998, **70**, 2651-2659.
- H. Gleiter, *Acta Materialia*, 2000, **48**, 1-29.
- J. V. Badding, *Annu. Rev. Mater. Sci.*, 1998, **28**, 631-658.
- C. N. R. Rao, *Mater. Sci. Eng. B*, 1993, **18**, 1-21.
- S. Parola, B. Julián-López, L. D. Carlos and C. Sanchez, *Adv. Funct. Mater.*, 2016, **26**, 6506-6544.
- L. Qiu, L. K. Ono and Y. Qi, *Mater. Today Energy*, 2018, **7**, 169-189.
- V. Fernandez-Moreira, F. L. Thorp-Greenwood and M. P. Coogan, *Chem. Commun.*, 2010, **46**, 186-202.

42. V. W. Yam, V. K. Au and S. Y. Leung, *Chem. Rev.*, 2015, **115**, 7589-7728.
43. D. Dini, M. J. Calvete and M. Hanack, *Chem. Rev.*, 2016, **116**, 13043-13233.
44. G. S. He, L. S. Tan, Q. Zheng and P. N. Prasad, *Chem. Rev.*, 2008, **108**, 1245-1330.
45. P. D. Beer, *Acc. Chem. Res.*, 1998, **31**, 71-80.
46. K. A. Green, M. P. Cifuentes, M. Samoc and M. G. Humphrey, *Coord. Chem. Rev.*, 2011, **255**, 2530-2541.
47. J. N. Demas and B. A. DeGraff, *Coord. Chem. Rev.*, 2001, **211**, 317-351.
48. C. K. Prier, D. A. Rankic and D. W. MacMillan, *Chem. Rev.*, 2013, **113**, 5322-5363.
49. R. Jana, T. P. Pathak and M. S. Sigman, *Chem. Rev.*, 2011, **111**, 1417-1492.
50. A. Z. Weber, M. M. Mench, J. P. Meyers, P. N. Ross, J. T. Gostick and Q. Liu, *J. Appl. Electrochem.*, 2011, **41**, 1137-1164.
51. S. Mecking, *Angew. Chem. Int. Ed.*, 2001, **40**, 534-540.
52. A. S. Abd-El-Aziz and I. Manners, *Frontiers in Transition Metal-Containing Polymers*, Wiley, 2006, DOI: 10.1002/0470086068.
53. K. L. Haas and K. J. Franz, *Chem. Rev.*, 2009, **109**, 4921-4960.
54. G. Gasser, I. Ott and N. Metzler-Nolte, *J. Med. Chem.*, 2011, **54**, 3-25.
55. D. C. Hone, P. I. Walker, R. Evans-Gowing, S. FitzGerald, A. Beeby, I. Chambrier, M. J. Cook and D. A. Russell, *Langmuir*, 2002, **18**, 2985-2987.
56. C. Quintana, M. Morshedi, H. Wang, J. Du, M. P. Cifuentes and M. G. Humphrey, *Nano Lett.*, 2019, **19**, 756-760.
57. S. D'Souza, S. Moeno, E. Antunes and T. Nyokong, *New J. Chem.*, 2013, **37**, 1950-1958.
58. L. Yang, N. Huang, Q. Lu, M. Liu, H. Li, Y. Zhang and S. Yao, *Anal. Chim. Acta*, 2016, **903**, 69-80.
59. T. Soller, M. Ringler, M. Wunderlich, T. A. Klar, J. Feldmann, H. P. Josel, Y. Markert, A. Nichtl and K. Kürzinger, *Nano Lett.*, 2007, **7**, 1941-1946.
60. Y. Kuwahara, T. Akiyama and S. Yamada, *Langmuir*, 2001, **17**, 5714-5716.
61. S. M. King, S. Claire, R. I. Teixeira, A. N. Dosumu, A. J. Carrod, H. Dehghani, M. J. Hannon, A. D. Ward, R. Bicknell, S. W. Botchway, N. J. Hodges and Z. Pikramenou, *J. Am. Chem. Soc.*, 2018, **140**, 10242-10249.
62. P. Garcia Calavia, G. Bruce, L. Perez-Garcia and D. A. Russell, *Photochem. Photobiol. Sci.*, 2018, **17**, 1534-1552.
63. N. Li, P. Zhao, M. E. Igartua, A. Rapakousiou, L. Salmon, S. Moya, J. Ruiz and D. Astruc, *Inorg. Chem.*, 2014, **53**, 11802-11808.
64. F. Liu, X. Liu, D. Astruc and H. Gu, *J. Coll. Interf. Sci.*, 2019, **533**, 161-170.
65. C. R. Mayer, E. Dumas and F. Secheresse, *J. Coll. Interf. Sci.*, 2008, **328**, 452-457.
66. X.-H. N. Xu, S. Huang, W. Brownlow, K. Salaita and R. B. Jeffers, *J. Phys. Chem. B*, 2004, **108**, 15543-15551.
67. R. N. Grimes, *Dalton Trans.*, 2015, **44**, 5939-5956.
68. M.-J. Li, X. Liu, M.-J. Nie, Z.-Z. Wu, C.-Q. Yi, G.-N. Chen and V. W.-W. Yam, *Organometallics*, 2012, **31**, 4459-4466.
69. N. Vilvamani, M. Chhatwal, I. Bhowmick, R. D. Gupta and S. K. Awasthi, *RSC Adv.*, 2016, **6**, 55507-55513.
70. P. Zhang, J. Wang, H. Huang, H. Chen, R. Guan, Y. Chen, L. Ji and H. Chao, *Biomaterials*, 2014, **35**, 9003-9011.
71. A. J. Jeevagan and S. A. John, *RSC Adv.*, 2013, **3**, 2256-2264.
72. C. Villena, M. Bravo, B. Alonso, C. M. Casado, J. Losada and M. P. García Armada, *Appl. Surf. Sci.*, 2017, **420**, 651-660.
73. T. P. Mthethwa, Y. Arslanoglu, E. Antunes and T. Nyokong, *Polyhedron*, 2012, **38**, 169-177.
74. E. Dube, D. O. Oluwole, E. Prinsloo and T. Nyokong, *New J. Chemistry*, 2018, **42**, 10214-10225.
75. N. Nombona, E. Antunes, C. Litwinski and T. Nyokong, *Dalton Trans.*, 2011, **40**, 11876-11884.
76. A. Mars, C. Parolo, N. Raouafi, K. Boujlel and A. Merkoçi, *J. Mater. Chem. B*, 2013, **1**, 2951-2955.
77. J. A. Robson, F. Gonzalez de Rivera, K. A. Jantan, M. N. Wenzel, A. J. White, O. Rossell and J. D. Wilton-Ely, *Inorg. Chem.*, 2016, **55**, 12982-12996.
78. E. R. Knight, N. H. Leung, A. L. Thompson, G. Hogarth and J. D. Wilton-Ely, *Inorg. Chem.*, 2009, **48**, 3866-3874.
79. S. Forteath, E. Antunes, W. Chidawanyika and T. Nyokong, *Polyhedron*, 2012, **34**, 114-120.
80. P. Zhang, J. Wang, H. Huang, B. Yu, K. Qiu, J. Huang, S. Wang, L. Jiang, G. Gasser, L. Ji and H. Chao, *Biomaterials*, 2015, **63**, 102-114.
81. F. Miomandre, S. Stancheva, J.-F. Audibert, A. Brosseau, R. B. Pansu, M. Lepeltier and C. R. Mayer, *J. Phys. Chem. C*, 2013, **117**, 12806-12814.
82. L. Guerret, J. F. Audibert, A. Debarre, M. Lepeltier, P. Haghi-Ashtiani, G. V. Dubacheva and F. Miomandre, *J. Phys. Chem. C*, 2016, **120**, 2411-2418.
83. T. P. Mthethwa, S. Tuncel, M. Durmus and T. Nyokong, *Dalton Trans.*, 2013, **42**, 4922-4930.
84. Y. Wang, L. Salmon, J. Ruiz and D. Astruc, *Nat. Commun.* 2014, **5**, 3489-3500.
85. Y. Liu, S. Mu, X. Liu, Q. Ling, C. Hang, J. Ruiz, D. Astruc and H. Gu, *Tetrahedron*, 2018, **74**, 4777-4789.
86. M. Friederici, I. Angurell, M. Seco, O. Rossell and J. Llorca, *Dalton Trans.*, 2011, **40**, 7934-7940.
87. F. González de Rivera, I. Angurell, O. Rossell, M. Seco and J. Llorca, *J. Organomet. Chem.*, 2012, **715**, 13-18.
88. M. Friederici, I. Angurell, O. Rossell, M. Seco and G. Muller, *J. Molec. Catal. A: Chem.*, 2013, **376**, 7-12.
89. A. J. Baca, F. Zhou, J. Wang, J. Hu, J. Li, J. Wang and Z. S. Chikneyan, *Electroanalysis*, 2004, **16**, 73-80.
90. J. D. Qiu, M. Xiong, R. P. Liang, H. P. Peng and F. Liu, *Biosens. Bioelectron.*, 2009, **24**, 2649-2653.
91. R. L. Stiles, R. Balasubramanian, S. W. Feldberg and R. W. Murray, *J. Am. Chem. Soc.*, 2008, **130**, 1856-1865.
92. W. Song, M. Okamura, T. Kondo and K. Uosaki, *J. Electroanal. Chem.*, 2003, **554-555**, 385-393.
93. C. D. Geddes and J. R. Lakowicz, *J. Fluorescence*, 2002, **12**, 121-129.
94. H. Shi, Y. Xu, Y. Wang and W. Song, *Microchim. Acta*, 2010, **171**, 81-89.
95. J.-D. Qiu, R. Wang, R.-P. Liang and M. Xiong, *Electroanalysis*, 2008, **20**, 1819-1824.

96. A. Daneshvar, M. Moghadam, S. Tangestaninejad, V. Mirkhani, I. Mohammadpoor-Baltork and A. Khalili, *Organometallics*, 2016, **35**, 1747-1755.
97. M. C. Martos-Maldonado, M. B. Thygesen, K. J. Jensen and A. Vargas-Berenguel, *Eur. J. Org. Chem.*, 2013, 2793-2801.
98. G. H. Woehrle, L. O. Brown and J. E. Hutchison, *J. Am. Chem. Soc.*, 2005, **127**, 2172-2183.
99. G. Nasr, A. Guerlin, F. Dumur, S. A. Baudron, E. Dumas, F. Miomandre, G. Clavier, M. Sliwa and C. R. Mayer, *J. Am. Chem. Soc.*, 2011, **133**, 6501-6504.
100. W. Song, M. Okamura, T. Kondo and K. Uosaki, *Phys. Chem. Chem. Phys.*, 2003, **5**, 5279-5284.
101. H. Hakkinen, *Nat. Chem.*, 2012, **4**, 443-455.
102. S. A. Osborne and Z. Pikramenou, *Faraday Discuss.*, 2015, **185**, 219-231.
103. N. J. Rogers, H. C. Jeffery, S. Claire, D. J. Lewis, G. Zikeli, N. J. Hodges, S. Egginton, G. B. Nash and Z. Pikramenou, *Nanomedicine*, 2017, **12**, 2725-2740.
104. R. B. Elmes, K. N. Orange, S. M. Cloonan, D. C. Williams and T. Gunnlaugsson, *J. Am. Chem. Soc.*, 2011, **133**, 15862-15865.
105. M. Martinez-Calvo, K. N. Orange, R. B. Elmes, B. la Cour Poulsen, D. C. Williams and T. Gunnlaugsson, *Nanoscale*, 2016, **8**, 563-574.
106. F. C.-M. Leung, V. K.-M. Au, H.-O. Song and V. W.-W. Yam, *Chem. Eur. J.*, 2015, **21**, 16448-16454.
107. F. C. Leung, A. Y. Tam, V. K. Au, M. J. Li and V. W. Yam, *ACS Appl. Mater. Interf.*, 2014, **6**, 6644-6653.
108. F. Vitale, R. Vitaliano, C. Battocchio, I. Fratoddi, C. Giannini, E. Piscopiello, A. Guagliardi, A. Cervellino, G. Polzonetti, M. V. Russo and L. Tapfer, *Nanoscale Res. Lett.*, 2008, **3**, 461-467.
109. F. Fu, Q. Wang, R. Ciganda, A. M. Martinez-Villacorta, A. Escobar, S. Moya, E. Fouquet, J. Ruiz and D. Astruc, *Chemistry*, 2018, **24**, 6645-6653.
110. R. Ciganda, H. Gu, R. Hernandez, A. Escobar, A. Martinez, L. Yates, S. Moya, J. Ruiz and D. Astruc, *Inorg. Chem.*, 2017, **56**, 2784-2791.
111. M. E. Alea-Reyes, J. Soriano, I. Mora-Espi, M. Rodrigues, D. A. Russell, L. Barrios and L. Perez-Garcia, *Coll. Surf. B Biointerfaces*, 2017, **158**, 602-609.
112. K. K.-W. Lo, M.-W. Louie and K. Y. Zhang, *Coord. Chem. Rev.*, 2010, **254**, 2603-2622.
113. V. Balzani, A. Juris, M. Venturi, S. Campagna and S. Serroni, *Chem. Rev.*, 1996, **96**, 759-834.
114. A. L. Noffke, A. Habtemariam, A. M. Pizarro and P. J. Sadler, *Chem. Commun.*, 2012, **48**, 5219-5246.
115. J. Turkevich, P. C. Stevenson and J. Hillier, *J. Phys. Chem.*, 1953, **57**, 670-673.
116. J. Kimling, M. Maier, B. Okenve, V. Kotaidis, H. Ballot and A. Plech, *J. Phys. Chem. B*, 2006, **110**, 15700-15707.
117. M. Brust, M. Walker, D. Bethell, D. J. Schiffrin and R. Whyman, *J. Chem. Soc., Chem. Commun.*, 1994, 801-802.
118. M. J. Hostetler, A. C. Templeton and R. W. Murray, *Langmuir*, 1999, **15**, 3782-3789.
119. H. E. Toma, V. M. Zamarion, S. H. Toma and K. Araki, *Braz. Chem. Soc.*, 2010, **21**, 1158-1176.
120. T. Yonezawa and T. Kunitake, *Coll. Surf. A*, 1999, **149**, 193-199.
121. C. Ziegler and A. Eychmüller, *J. Phys. Chem. C*, 2011, **115**, 4502-4506.
122. R. Ciganda, J. Irigoyen, D. Gregurec, R. Hernandez, S. Moya, C. Wang, J. Ruiz and D. Astruc, *Inorg. Chem.*, 2016, **55**, 6361-6363.
123. P. Garcia Calavia, M. J. Marin, I. Chambrier, M. J. Cook and D. A. Russell, *Photochem. Photobiol. Sci.*, 2018, **17**, 281-289.
124. M. Camerin, M. Moreno, M. J. Marin, C. L. Schofield, I. Chambrier, M. J. Cook, O. Coppellotti, G. Jori and D. A. Russell, *Photochem. Photobiol. Sci.*, 2016, **15**, 618-625.
125. L. Zhai and R. D. McCullough, *J. Mater. Chem.*, 2004, **14**, 141-143.
126. M. E. Wieder, D. C. Hone, M. J. Cook, M. M. Handsley, J. Gavrilovic and D. A. Russell, *Photochem. Photobiol. Sci.*, 2006, **5**, 727-734.
127. J. Wang, J. Li, A. J. Baca, J. Hu, F. Zhou, W. Yan and D.-W. Pang, *Anal. Chem.*, 2003, **75**, 3941-3945.
128. M. E. Alea-Reyes, O. Penon, P. Garcia Calavia, M. J. Marin, D. A. Russell and L. Perez-Garcia, *J. Coll. Interf. Sci.*, 2018, **521**, 81-90.
129. A. J. Hallett, P. Christian, J. E. Jones and S. J. Pope, *Chem. Commun.*, 2009, 4278-4280.
130. T. Huang and R. W. Murray, *Langmuir*, 2002, **18**, 7077-7081.
131. N. J. Rogers, S. Claire, R. M. Harris, S. Farabi, G. Zikeli, I. B. Styles, N. J. Hodges and Z. Pikramenou, *Chem. Commun.*, 2014, **50**, 617-619.
132. F. Chen, X. Li, J. Hihath, Z. Huang and N. Tao, *J. Am. Chem. Soc.*, 2006, **128**, 15874-15881.
133. P. Pramod, P. K. Sudeep, K. G. Thomas and P. V. Kamat, *J. Phys. Chem. B*, 2006, **110**, 20737-20741.
134. A. Rapakousiou, R. Djeda, M. Grillaud, N. Li, J. Ruiz and D. Astruc, *Organometallics*, 2014, **33**, 6953-6962.
135. O. M. Bankole and T. Nyokong, *J. Mol. Struct.*, 2017, **1136**, 309-320.
136. L. Pérez-Mirabet, S. Surinyach, J. Ros, J. Suades and R. Yáñez, *Mater. Chem. Phys.*, 2012, **137**, 439-447.
137. W. R. Glomm, S. J. Moses, M. K. Brennaman, J. M. Papanikolas and S. Franzen, *J. Phys. Chem. B*, 2005, **109**, 804-810.
138. M. M. Modena, B. Rühle, T. P. Burg and S. Wuttke, *Adv. Mater.*, 2019, 1901556-1901582.
139. W. Haiss, N. T. Thanh, J. Aveyard and D. G. Fernig, *Anal. Chem.*, 2007, **79**, 4215-4221.
140. E. V. Orlova and H. R. Saibil, *Chem. Rev.*, 2011, **111**, 7710-7748.
141. E. Buhr, N. Senftleben, T. Klein, D. Bergmann, D. Gnieser, C. G. Frase and H. Bosse, *Meas. Sci. Technol.*, 2009, **20**, 084025-084034.
142. E. Pensa, E. Cortés, G. Corthey, P. Carro, C. Vericat, M. H. Fonticelli, G. Benítez, A. A. Rubert and R. C. Salvarezza, *Acc. Chem. Res.*, 2012, **45**, 1183-1192.
143. T. Zheng, S. Bott and Q. Huo, *ACS Appl. Mater. Interf.*, 2016, **8**, 21585-21594.
144. A. M. Smith, L. E. Marbella, K. A. Johnston, M. J. Hartmann, S. E. Crawford, L. M. Kozycz, D. S. Seferos and J. E. Millstone, *Anal. Chem.*, 2015, **87**, 2771-2778.
145. R. Allabashi, W. Stach, A. de la Escosura-Muñiz, L. Liste-Calleja and A. Merkoçi, *J. Nanopart. Res.*, 2008, **11**, 2003-2011.

146. S. Elzey, D. H. Tsai, S. A. Rabb, L. L. Yu, M. R. Winchester and V. A. Hackley, *Anal. Bioanal. Chem.*, 2012, **403**, 145-149.
147. E. Mansfield, K. M. Tyner, C. M. Poling and J. L. Blacklock, *Anal. Chem.*, 2014, **86**, 1478-1484.
148. T. Burgi, *Nanoscale*, 2015, **7**, 15553-15567.
149. J. Yang, E. H. Sargent, S. O. Kelley and J. Y. Ying, *Nat. Mater.*, 2009, **8**, 683-689.
150. V. A. Dhumale, R. K. Gangwar, S. S. Datar and R. B. Sharma, *Mater. Express*, 2012, **2**, 311-318.
151. G. Jiang, L. Wang and W. Chen, *Mater. Lett.*, 2007, **61**, 278-283.
152. A. Kumar, S. Mandal, P. R. Selvakannan, R. Pasricha, A. B. Mandale and M. Sastry, *Langmuir*, 2003, **19**, 6277-6282.
153. P. Zhang and T. K. Sham, *Phys. Rev. Lett.*, 2003, **90**, 2455021-2455024.
154. T. L. Doane, C. H. Chuang, R. J. Hill and C. Burda, *Acc. Chem. Res.*, 2012, **45**, 317-326.
155. J. F. Li, Y. J. Zhang, S. Y. Ding, R. Panneerselvam and Z. Q. Tian, *Chem. Rev.*, 2017, **117**, 5002-5069.
156. M. Ben Haddada, J. Blanchard, S. Casale, J.-M. Krafft, A. Vallée, C. Méthivier and S. Boujday, *Gold Bull.*, 2013, **46**, 335-341.
157. R. Szatanek, M. Baj-Krzyworzeka, J. Zimoch, M. Lekka, M. Siedlar and J. Baran, *Int. J. Mol. Sci.*, 2017, **18**.
158. O. Osifeko and T. Nyokong, *Dyes Pigm.*, 2016, **131**, 186-200.
159. S. Link and M. A. El-Sayed, *J. Phys. Chem. B*, 1999, **103**, 4212-4217.
160. D. V. Leff, L. Brandt and J. R. Heath, *Langmuir*, 1996, **12**, 4723-4730.
161. A. Liese and L. Hilterhaus, *Chem. Soc. Rev.*, 2013, **42**, 6236-6249.
162. L. Trapiella-Alfonso, J. M. Costa-Fernández, J. Ruiz-Encinar, R. Pereiro and A. Sanz-Medel, *Mass Spectrometry for the Characterization of Gold Nanoparticles*, Elsevier, 2014, ch. 8, DOI: 10.1016/B978-0-444-63285-2.00008-0.
163. X. Liu, M. Atwater, J. Wang and Q. Huo, *Coll. Surf. B: Biointerf.*, 2007, **58**, 3-7.
164. C. Quintana, M. Morshedi, J. P. L. Morrall, J. K. Zaręba, M. Samoć, M. P. Cifuentes and M. G. Humphrey, submitted.
165. K. Aslan, I. Gryczynski, J. Malicka, E. Matveeva, J. R. Lakowicz and C. D. Geddes, *Curr. Opin. Biotechnol.*, 2005, **16**, 55-62.
166. T. J. Penfold, E. Gindensperger, C. Daniel and C. M. Marian, *Chem. Rev.*, 2018, **118**, 6975-7025.
167. P. K. Jain, X. Huang, I. H. El-Sayed and M. A. El-Sayed, *Plasmonics*, 2007, **2**, 107-118.
168. M. Swierczewska, S. Lee and X. Chen, *Phys. Chem. Chem. Phys.*, 2011, **13**, 9929-9941.
169. P. K. Jain, W. Huang and M. A. El-Sayed, *Nano Lett.*, 2007, **7**, 2080-2088.
170. K. Nakamaru, *Bull. Chem. Soc. Jpn.*, 1982, **55**, 2697-2705.
171. P. Bertoncello, E. T. Kefalas, Z. Pikramenou, P. R. Unwin and R. J. Forster, *J. Phys. Chem. B*, 2006, **110**, 10063-10069.
172. S. J. Adams, D. J. Lewis, J. A. Preece and Z. Pikramenou, *ACS Appl. Mater. Interf.*, 2014, **6**, 11598-11608.
173. V. V. Sapunov and G. D. Egorova, *J. Appl. Spectrosc.*, 1991, **54**, 427-432.
174. X. H. Cao, Q. Wang, J. Li, C. Q. Yi and M. J. Li, *Microchim. Acta*, 2017, **184**, 3273-3279.
175. D. Astruc, *Eur. J. Inorg. Chem.*, 2017, 6-29.
176. S. J. Green, J. J. Stokes, M. J. Hostetler, J. Pietron and R. W. Murray, *J. Phys. Chem. B*, 1997, **101**, 2663-2668.
177. M. J. Hostetler, S. J. Green, J. J. Stokes and R. W. Murray, *J. Am. Chem. Soc.*, 1996, **118**, 4212-4213.
178. R. H. Terrill, T. A. Postlethwaite, C. Chen, C. Poon, A. Terzis, A. Chen, J. E. Hutchison, M. R. Clark and G. Wignall, *J. Am. Chem. Soc.*, 1995, **117**, 12537-12548.
179. R. L. Wolfe, R. Balasubramanian, J. B. Tracy and R. W. Murray, *Langmuir*, 2007, **23**, 2247-2254.
180. A. J. Baca, F. Zhou, J. Wang, J. Hu, J. Li, J. Wang and Z. S. Chikneyan, *Electroanalysis*, 2004, **16**, 73-80.
181. M. Yamada, T. Tadera, K. Kubo and H. Nishihara, *J. Phys. Chem. B*, 2003, **107**, 3703-3711.
182. M. Yamada and H. Nishihara, *Langmuir*, 2003, **19**, 8050-8056.
183. M. Yamada and H. Nishihara, *Eur. Phys. J. D – Atom. Molec. Opt. Phys.*, 2003, **24**, 257-260.
184. T. Horikoshi, M. Itoh, M. Kurihara, K. Kubo and H. Nishihara, *J. Electroanal. Chem.*, 1999, **473**, 113-116.
185. M. Yamada and H. Nishihara, *C. R. Chim.*, 2003, **6**, 919-934.
186. T.-Y. Dong, L.-S. Chang, I. M. Tseng and S.-J. Huang, *Langmuir*, 2004, **20**, 4471-4479.
187. Y. Men, K. Kubo, M. Kurihara and H. Nishihara, *Phys. Chem. Chem. Phys.*, 2001, **3**, 3427-3430.
188. H.-W. Shih and T.-Y. Dong, *Inorg. Chem. Commun.*, 2004, **7**, 646-649.
189. D. Li, Y. Zhang, J. Jiang and J. Li, *J. Coll. Interf. Sci.*, 2003, **264**, 109-113.
190. R. M. Choueiri, A. Klinkova, S. Pearce, I. Manners and E. Kumacheva, *Macromol. Rapid. Commun.*, 2018, **39**, 1700554.
191. M.-C. Daniel, J. R. Aranzaes, S. Nlate and D. Astruc, *J. Inorg. Organomet. Polym. Mater.*, 2005, **15**, 107-119.
192. M. C. Daniel, J. Ruiz, S. Nlate, J. C. Blais and D. Astruc, *J. Am. Chem. Soc.*, 2003, **125**, 2617-2628.
193. M. Yamada and H. Nishihara, *Langmuir*, 2003, **19**, 8050-8056.
194. M. Liu, Q. Chen, C. Lai, Y. Zhang, J. Deng, H. Li and S. Yao, *Biosens. Bioelectron.*, 2013, **48**, 75-81.
195. M.-C. Daniel, J. Ruiz, S. Nlate, J. Palumbo, D. Astruc and J.-C. Blais, *Chem. Commun.*, 2001, 2000-2001.
196. G. M. Farinola and R. Ragni, *Chem. Soc. Rev.*, 2011, **40**, 3467-3482.
197. G. M. Calixto, J. Bernegossi, L. M. de Freitas, C. R. Fontana and M. Chorilli, *Molecules*, 2016, **21**, 342-360.
198. R. R. Allison and C. H. Sibata, *Photodiag. Photodyn. Ther.*, 2010, **7**, 61-75.
199. Y. Zhang and J. F. Lovell, *WIREs Nanomed. Nanobiotechnol.*, 2017, **9**, 1-15.
200. R. Bonnett, *Chem. Soc. Rev.*, 1995, **24**, 19-33.
201. C. Yao, L. Zhang, J. Wang, Y. He, J. Xin, S. Wang, H. Xu and Z. Zhang, *J. Nanomat.*, 2016, **2016**, 1-29.
202. Y. Cheng, T. L. Doane, C. H. Chuang, A. Ziady and C. Burda, *Small*, 2014, **10**, 1799-1804.

203. X. Chen, Q. Ye, D. Ma, J. Chen, Y. Wang, H. Yang, S. Xie, R. Yu and Y. Peng, *J. Luminescence*, 2018, **195**, 348-355.
204. S. Moeno, E. Antunes and T. Nyokong, *J. Photochem. Photobiol. A: Chem.*, 2011, **222**, 343-350.
205. M. Camerin, M. Magaraggia, M. Soncin, G. Jori, M. Moreno, I. Chambrier, M. J. Cook and D. A. Russell, *Eur. J. Cancer*, 2010, **46**, 1910-1918.
206. A. V. Zasedatelev, T. V. Dubinina, D. M. Krichevsky, V. I. Krasovskii, V. Y. Gak, V. E. Pushkarev, L. G. Tomilova and A. A. Chistyakov, *J. Phys. Chem. C*, 2016, **120**, 1816-1823.
207. L. W. Tutt and T. F. Boggess, *Progr. Quant. Electron.*, 1993, **17**, 299-338.
208. H. M. Kim and B. R. Cho, *Chem. Rev.*, 2015, **115**, 5014-5055.
209. G. Chen, I. Roy, C. Yang and P. N. Prasad, *Chem. Rev.*, 2016, **116**, 2826-2885.
210. J. Olesiak-Banska, M. Waszkielewicz, P. Obstarczyk and M. Samoc, *Chem. Soc. Rev.*, 2019, **48**, 4087-4117.
211. Y.-X. Zhang and Y.-H. Wang, *RSC Adv.*, 2017, **7**, 45129-45144.
212. V. Amendola, D. Dini, S. Polizzi, J. Shen, K. M. Kadish, M. J. F. Calvete, M. Hanack and M. Meneghetti, *J. Phys. Chem. C*, 2009, **113**, 8688-8695.
213. Q. Zhang, X. Tian, H. Zhou, J. Wu and Y. Tian, *Materials*, 2017, **10**, 223-260.
214. M. Samoc, N. Gauthier, M. P. Cifuentes, F. Paul, C. Lapinte and M. G. Humphrey, *Angew. Chem. Int. Ed.*, 2006, **45**, 7376-7379.
215. P. V. Simpson, L. A. Watson, A. Barlow, G. Wang, M. P. Cifuentes and M. G. Humphrey, *Angew. Chem. Int. Ed.*, 2016, **128**, 2433-2437.
216. G. J. Zhou and W. Y. Wong, *Chem. Soc. Rev.*, 2011, **40**, 2541-2566.
217. B. Gao, L. M. Mazur, M. Morshedi, A. Barlow, H. Wang, C. Quintana, C. Zhang, M. Samoc, M. P. Cifuentes and M. G. Humphrey, *Chem. Commun.*, 2016, **52**, 8301-8304.
218. J. Moreau, F. Lux, M. Four, J. Olesiak-Banska, K. Matczyszyn, P. Perriat, C. Frochot, P. Arnoux, O. Tillement, M. Samoc, G. Ponterini, S. Roux and G. Lemerrier, *Phys. Chem. Chem. Phys.*, 2014, **16**, 14826-14833.
219. G. Lemerrier, M. Four and S. Chevreux, *Coord. Chem. Rev.*, 2018, **368**, 1-12.
220. B. S. Takale, M. Bao and Y. Yamamoto, *Org. Biomol. Chem.*, 2014, **12**, 2005-2027.
221. H. Chao, R.-H. Li, C.-W. Jiang, H. Li, L.-N. Ji and X.-Y. Li, *J. Chem. Soc., Dalton Trans.*, 2001, 1920-1926.
222. D. T. Thompson, *Nano Today*, 2007, **2**, 40-43.
223. J. D. E. T. Wilton-Ely, *Dalton Trans.*, 2008, 25-29.



Cristóbal Quintana is completing doctoral studies in the group of Prof. Mark G. Humphrey at the Australian National University, Australia. He received his BSc in 2014 from the Pontificia Universidad Católica de Valparaíso, Chile, majoring in chemistry. His current research interests focus on hybrid organometallic materials for nonlinear optics.



Marie P. Cifuentes received a PhD from the University of New England (Australia), and has held three Fellowships from the Australian Research Council at the Research School of Chemistry at ANU. She has been an Associate Professor at RSC since 2015, and she is the author of ca. 170 papers dealing with various aspects of organometallic chemistry.



Mark G. Humphrey received PhD and DSc degrees from the University of Adelaide (Australia) and a DUniv (h.c.) from Université Rennes 1 (France). He was appointed Professor at the Research School of Chemistry at ANU in 2003, and he is the author of ca. 340 publications dealing with organometallic and materials chemistry.